1
Artificial Photochemical Devices and Machines

Vincenzo Balzani, Alberto Credi, and Margherita Venturi

1.1
Introduction

The interaction between light and matter lies at the heart of the most important processes of life [1]. Photons are exploited by natural systems as both quanta of energy and elements of information. Light constitutes an energy source and is consumed (or, more precisely, converted) in large amount in the natural photosynthetic process, whereas it plays the role of a signal in vision-related processes, where the energy used to run the operation is biological in nature.

A variety of functions can also be obtained from the interaction between light and matter in artificial systems [2]. The type and utility of such functions depend on the degree of complexity and organization of the chemical systems that receive and process the photons.

About 20 years ago, in the frame of research on supramolecular chemistry, the idea began to arise [3–5] that the concept of macroscopic device and machine can be transferred to the molecular level. In short, a molecular device can be defined [6] as an assembly of a discrete number of molecular components designed to perform a function under appropriate external stimulation. A molecular machine [6–8] is a particular type of device where the function is achieved through the mechanical movements of its molecular components.

In analogy with their macroscopic counterparts, molecular devices and machines need energy to operate and signal to communicate with the operator. Light provides an answer to this dual requirement. Indeed, a great number of molecular devices and machines are powered by light-induced processes and light can also be useful to "read" the state of the system and thus to control and monitor its operation. Before illustrating examples of artificial photochemical molecular devices and machines, it is worthwhile recalling a few basic aspects of the interaction between molecular and supramolecular systems and light. For a more detailed discussion, books [9–15] can be consulted.

Organic Nanostructures. Edited by Jerry L. Atwood and Jonathan W. Steed

ISBN: 978-3-527-31836-0

1.2
Molecular and Supramolecular Photochemistry

1.2.1
Molecular Photochemistry

Figure 1.1 shows a schematic energy level diagram for a generic molecule that could also be a component of a supramolecular species. In most cases the ground state of a molecule is a singlet state (S_0) and the excited states are either singlets (S_1, S_2, etc.) or triplets (T_1, T_2, etc.). In principle, transitions between states having the same spin value are allowed, whereas those between states of different spin are forbidden. Therefore, the electronic absorption bands observed in the UV–visible spectrum of molecules usually correspond to $S_0 \rightarrow S_n$ transitions. The excited states so obtained are unstable species that decay by rapid first-order kinetic processes, namely chemical reactions (e.g. dissociation, isomerization) and/or radiative and nonradiative deactivations. In the discussion that follows, excited-state reactions do not need to be explicitly considered and can formally be incorporated within the radiationless decay processes. When a molecule is excited to upper singlet excited states (Figure 1.1), it usually undergoes a rapid and 100% efficient radiationless deactivation [internal conversion (ic)] to the lowest excited singlet, S_1. Such an excited state undergoes deactivation via three competing processes: nonradiative decay to the ground state (internal conversion, rate constant k_{ic}); radiative decay to the ground state (fluorescence, k_{fl}); conversion to the lowest triplet state T_1 (intersystem crossing, k_{isc}). In its turn, T_1 can undergo deactivation via nonradiative (intersystem crossing, k'_{isc}) or radiative (phosphorescence, k_{ph}) decay to the ground state S_0. When the molecule contains heavy atoms, the formally forbidden intersystem crossing and

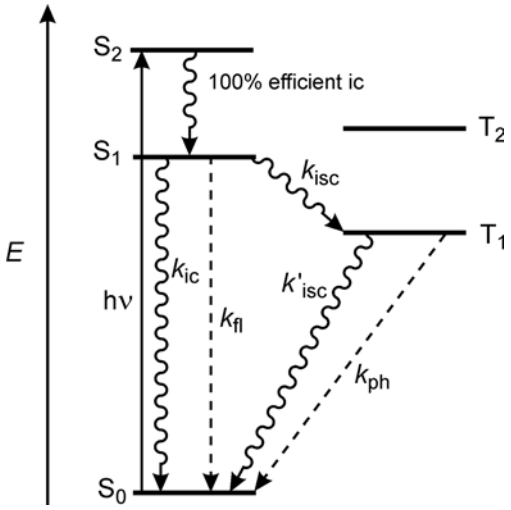

Figure 1.1 Schematic energy level diagram for a generic molecule. For more details, see text.

phosphorescence processes become faster. The lifetime (τ) of an excited state, that is, the time needed to reduce the excited-state concentration by 2.718 (i.e. the basis for natural logarithms, e), is given by the reciprocal of the summation of the deactivation rate constants:

$$\tau(S_1) = \frac{1}{(k_{ic}+k_{fl}+k_{isc})} \tag{1}$$

$$\tau(T_1) = \frac{1}{(k'_{isc}+k_{ph})} \tag{2}$$

The orders of magnitude of $\tau(S_1)$ and $\tau(T_1)$ are approximately $10^{-9}-10^{-7}$ and $10^{-3}-10^{0}$ s, respectively. The quantum yield of fluorescence (ratio between the number of photons emitted by S_1 and the number of absorbed photons) and phosphorescence (ratio between the number of photons emitted by T_1 and the number of absorbed photons) can range between 0 and 1 and are given by

$$\Phi_{fl} = \frac{k_{fl}}{(k_{ic}+k_{fl}+k_{isc})} \tag{3}$$

$$\Phi_{ph} = \frac{k_{ph} \times k_{isc}}{(k'_{isc}+k_{ph}) \times (k_{ic}+k_{fl}+k_{isc})} \tag{4}$$

Excited-state lifetimes and fluorescence and phosphorescence quantum yields of a great number of molecules are known [16].

When the intramolecular deactivation processes are not too fast, that is, when the lifetime of the excited state is sufficiently long, an excited molecule $^*A$ may have a chance to encounter a molecule of another solute, B (Figure 1.2). In such a case, some specific interaction can occur leading to the deactivation of the excited state by second-order kinetic processes. The two most important types of interactions in an encounter are those leading to electron or energy transfer. The occurrence of these processes causes the quenching of the intrinsic properties of $^*A$; energy transfer also

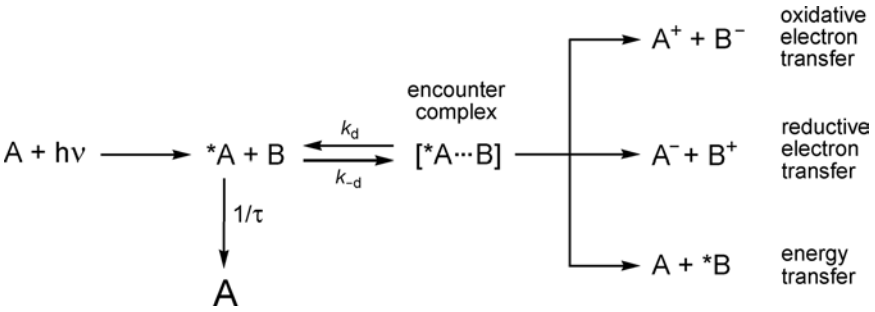

Figure 1.2 Schematic representation of bimolecular electron- and energy-transfer processes that may occur following an encounter between an excited state, $^*A$, and another chemical species, B.

leads to sensitization of the excited-state properties of the B species. Simple kinetic arguments show that only the excited states that live longer than ca. 10^{-9} s may have a chance to be involved in encounters with other solute molecules.

An electronically excited state is a species with completely different properties to those of the ground-state molecule. In particular, because of its higher energy content, an excited state is both a stronger reductant and a stronger oxidant than the corresponding ground state [17]. To a first approximation, the redox potential of an excited-state couple may be calculated from the potential of the related ground-state couple and the one-electron potential corresponding to the zero–zero excited-state energy, $E^{0\text{–}0}$:

$$E(A^+/{}^*A) \approx E(A^+/A) - E^{0\text{–}0} \tag{5}$$

$$E({}^*A/A^-) \approx E(A/A^-) + E^{0\text{–}0} \tag{6}$$

Detailed discussions of the kinetics aspects of electron- and energy-transfer processes can be found in the literature [11,18–20].

1.2.2 Supramolecular Photochemistry

A supramolecular system can be preorganized so as to favor the occurrence of electron- and energy-transfer processes [10]. The molecule that has to be excited, A, can indeed be placed in the supramolecular structure nearby a suitable molecule, B.

For simplicity, we consider the case of an A–L–B supramolecular system, where A is the light-absorbing molecular unit [Eq. (7)], B is the other molecular unit involved with A in the light-induced processes and L is a connecting unit (often called bridge). In such a system, after light excitation of A there is no need to wait for a diffusion-controlled encounter between *A and B as in molecular photochemistry, since the two reaction partners can already be at an interaction distance suitable for electron and energy transfer:

$$A{-}L{-}B + h\nu \rightarrow {}^*A{-}L{-}B \qquad \text{photoexcitation} \tag{7}$$

$${}^*A{-}L{-}B \rightarrow A^+{-}L{-}B^- \qquad \text{oxidative electron transfer} \tag{8}$$

$${}^*A{-}L{-}B \rightarrow A^-{-}L{-}B^+ \qquad \text{reductive electron transfer} \tag{9}$$

$${}^*A{-}L{-}B \rightarrow A{-}L{-}{}^*B \qquad \text{electronic energy transfer} \tag{10}$$

In the absence of chemical complications (e.g. fast decomposition of the oxidized and/or reduced species), photoinduced electron-transfer processes [Eqs. (8) and (9)] are followed by spontaneous back-electron-transfer reactions that regenerate the starting ground-state system [Eqs. 8′ and 9′] and photoinduced energy transfer [Eq. (10)] is followed by radiative and/or nonradiative deactivation of the excited acceptor [Eq. 10′]:

$$A^+{-}L{-}B^- \rightarrow A{-}L{-}B \qquad \text{back oxidative electron transfer} \tag{8′}$$

$$A^- - L - B^+ \rightarrow A - L - B \qquad \text{back reductive electron transfer} \qquad (9')$$

$$A - L - {}^*B \rightarrow A - L - B \qquad \text{excited state decay} \qquad (10')$$

In supramolecular systems, electron- and energy-transfer processes are no longer limited by diffusion and occur by first-order kinetics. As a consequence, in suitably designed supramolecular systems these processes can involve even very short-lived excited states.

1.3
Wire-Type Systems

An important function at the molecular level is photoinduced energy and electron transfer over long distances and/or along predetermined directions. This function can be performed by rod-like supramolecular systems obtained by linking donor and acceptor components with a bridging ligand or a spacer.

1.3.1
Molecular Wires for Photoinduced Electron Transfer

Photoinduced electron transfer in wire-type supramolecular species has been extensively investigated [6,10]. The minimum model is a *dyad*, consisting of an electron donor (or acceptor) chromophore, an additional electron acceptor (or donor) moiety and an organizational principle that controls their distance and electronic interactions (and therefore the rates and yields of electron transfer). A great number of such dyads have been constructed and investigated [6,10].

The energy-level diagram for a dyad is schematized in Figure 1.3. All the dyad-type systems suffer to a greater or lesser extent from rapid charge recombination

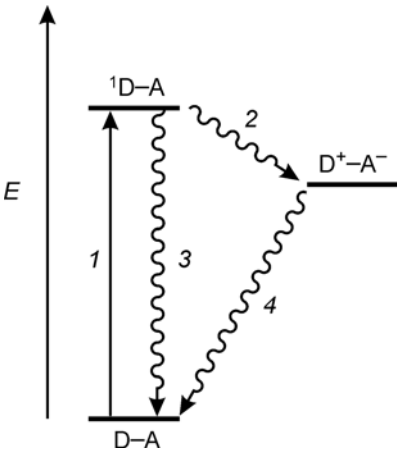

Figure 1.3 Schematic energy-level diagram for a dyad.

[process (4)]. An example of a systematic study on dyads is that performed on compounds $\mathbf{1}^{5+}$–$\mathbf{5}^{5+}$ (Figure 1.4) [21,22]. When excitation is selectively performed in the Ru(II) chromophoric unit, prompt intersystem crossing from the originally populated singlet metal-to-ligand charge-transfer (^{1}MLCT) excited state leads to the long-lived ^{3}MLCT excited state which lies ~2.1 eV above the ground state, can be oxidized approximately at −0.9 V (vs. SCE) and has a lifetime of ~1 μs in deaerated solutions [23]. Before undergoing deactivation, such an excited state transfers an electron to the Rh(III) unit, a process that is then followed by a back electron-transfer reaction.

Comparison of compounds $\mathbf{1}^{5+}$ and $\mathbf{2}^{5+}$ shows that, despite the longer metal–metal distance, the forward electron transfer is faster across the phenylene spacer ($k = 3.0 \times 10^9\ s^{-1}$) than across the two methylene groups ($k = 1.7 \times 10^8\ s^{-1}$). This result can be related to the lower energy of the LUMO of the phenylene group, which facilitates electronic coupling. In the homogeneous family of compounds $\mathbf{2}^{5+}$–$\mathbf{4}^{5+}$, the rate constant decreases exponentially with increasing metal–metal distance.

For compound $\mathbf{5}^{5+}$, which is identical with $\mathbf{4}^{5+}$ except for the presence of two solubilizing hexyl groups on the central phenylene ring, the photoinduced electron-transfer process is 10 times slower, presumably because the substituents increase the twist angle between the phenylene units, thereby reducing electronic coupling.

Photoinduced electron transfer in three–component systems (*triads*) is illustrated in Figure 1.5 [24]. The functioning principles are shown in the orbital-type energy diagrams of the lower part the figure. In both cases, excitation of a chromophoric component (step *1*) is followed by a primary photoinduced electron transfer to a primary acceptor (step *2*). This process is followed by a secondary thermal electron-transfer process (step *3*): electron transfer from a donor component to the oxidized chromophoric component (case a) or electron transfer from the primary acceptor to a secondary acceptor component (case b). The primary process competes with excited-state deactivation (step *4*), whereas the secondary process competes with primary charge recombination (step *5*). Finally, charge recombination between remote molecular components (step *6*) leads the triad back to its initial state.

For case a, the sequence of processes indicated above (*1–2–3*) is not unique. Actually, the alternative sequence *1–3–2* would also lead to the same charge-separated state. In general, these two pathways will have different driving forces for the primary and secondary steps and thus one may be kinetically favored over the other. Occasionally one of the two pathways is thermodynamically allowed and the other is not, although in a simple one-electron energy diagram like that shown in Figure 1.5a this aspect is not apparent.

The performance of a triad for wire-type applications is related to the rate and quantum yield of formation of the charge separated state (depending on the competition between forward and back processes, $\Phi = [k_2/(k_2 + k_4)][k_3/(k_3 + k_5)]$). For energy conversion purposes, important parameters are also the lifetime of charge separation (depending on the rate of the final charge-recombination process, $\tau = 1/k_6$) and the efficiency of energy conversion ($\eta_{en.conv.} = \Phi \times F$, where F is the fraction of the excited-state energy conserved in the final charge-separated state). To put things in a real perspective, it should be recalled that the "triad portion" of the

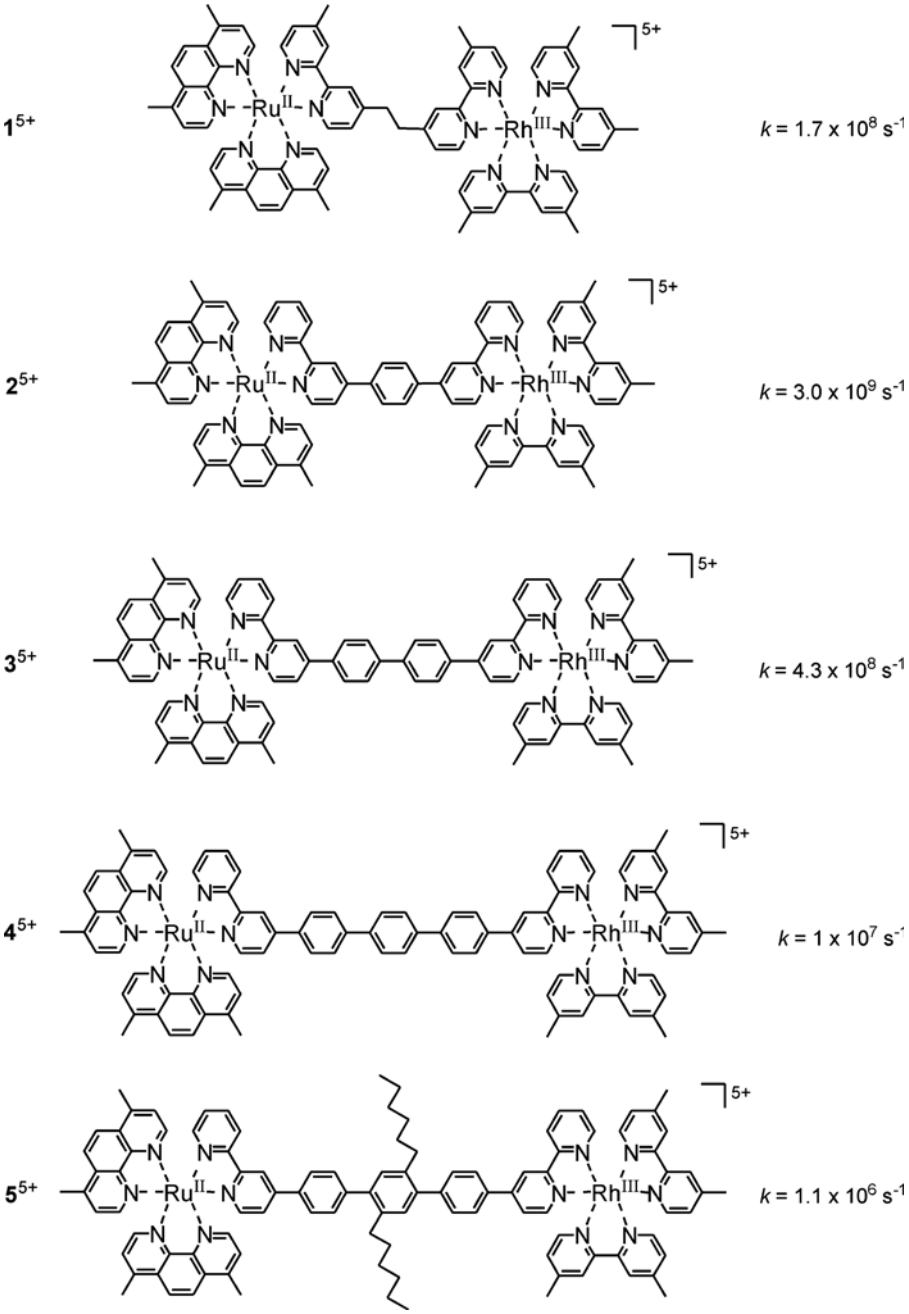

Figure 1.4 Binuclear metal complexes $\mathbf{1}^{5+}$–$\mathbf{5}^{5+}$ used for photoinduced electron-transfer experiments [21,22].

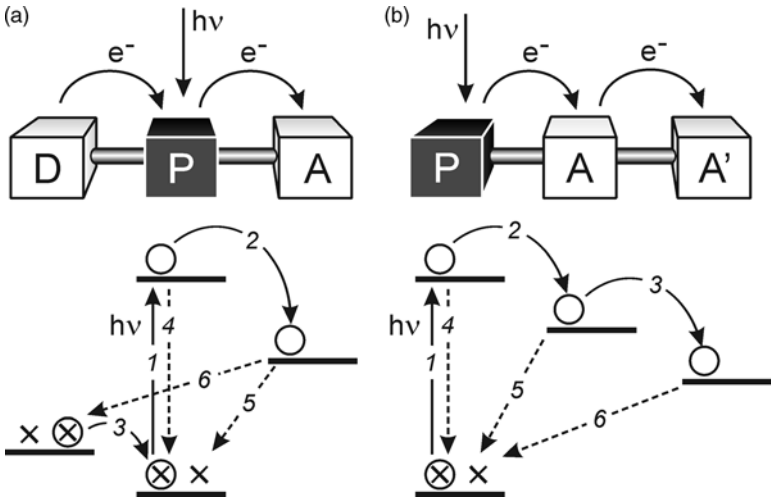

Figure 1.5 Schematic representation of the two possible arrangements for charge-separating triads.

reaction center of bacterial photosynthesis converts light energy with $\tau \approx 10\,\text{ms}$, $\Phi = 1$ and $\eta_{\text{en.conv.}} \approx 0.6$.

The introduction of further molecular components (*tetrads* and *pentads*) leads to the occurrence of further electron-transfer steps, which, in suitably designed systems, produce charge separation over larger and larger distances [6,10]. As the number of molecular components increases, also the mechanistic complexity increases and charge separation may involve energy-transfer steps.

Several triads have been designed and investigated. A very interesting system is the 4-nm long triad $\mathbf{6}^{3+}$ shown in Figure 1.6, which consists of an Ir(III) bis-terpyridine

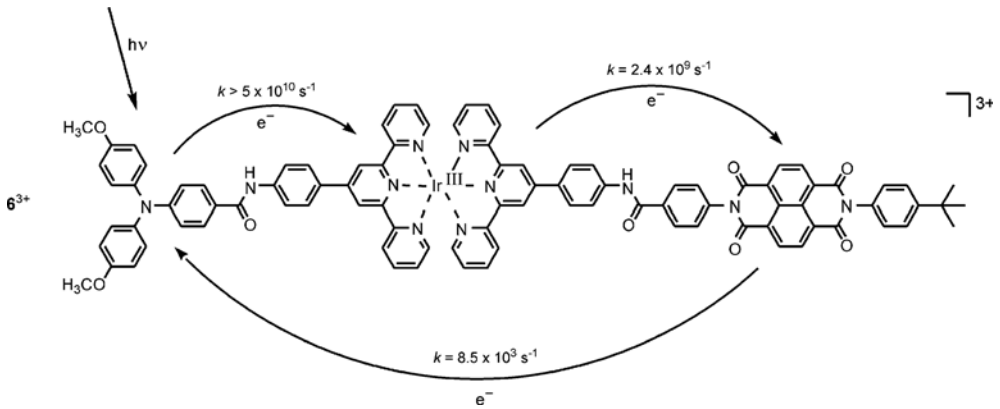

Figure 1.6 Electron-transfer processes in triad $\mathbf{6}^{3+}$ [25].

complex connected to a triphenylamine electron donor (D) and a naphthalene bisimide electron acceptor (A) [25]. Upon excitation of the electron donor D (or even the Ir-based moiety), a charge separated state D^+–Ir^-–A is formed with 100% yield in less than 20 ps that successively leads to D^+–Ir–A^- with 10% efficiency in 400 ps. Remarkably, the fully charge-separated state D^+–Ir–A^- has a lifetime of 120 μs at room temperature in deaerated acetonitrile solution.

1.3.2
Molecular Wires for Photoinduced Energy Transfer

Many investigations on electronic energy transfer in supramolecular species have been performed in the past few years [6,10], a relevant fraction of which have been obtained for systems containing polypyridine metal complexes as donor and acceptor units. Usually, the photoexcited chromophoric group is $[Ru(bpy)_3]^{2+}$ (bpy = 2,2′-bipyridine) and the energy acceptor is an $[Os(bpy)_3]^{2+}$ unit. The excited state of $[Ru(bpy)_3]^{2+}$ playing the role of energy donor is the lowest, formally triplet, metal-to-ligand charge-transfer excited state, ^{3}MLCT, which, as we have seen above, can be obtained by visible light excitation ($\lambda_{max} \approx 450$ nm), lies ~2.1 eV above the ground state and has a lifetime of ~1 μs in deaerated solutions [23]. This relatively long lifetime is very useful because it permits the study of energy transfer over long distances. The occurrence of the energy-transfer process promotes the ground-state $[Os(bpy)_3]^{2+}$ acceptor unit to its lowest energy excited state ^{3}MLCT, which lies approximately 0.35 eV below the donor excited state. Both the donor and the acceptor excited states are luminescent, so that the occurrence of energy transfer can be monitored by quenching and/or sensitization experiments with both continuous and pulsed excitation techniques.

Ru(II) and Os(II) polypyridine units have been connected by a variety of bridging ligands and spacers. When the metal-to-metal distance is very short, fast energy transfer occurs by a Förster-type resonance mechanism [26]. In other systems the two photoactive units are separated by a more or less long spacer. When the spacer is flexible [e.g. $-(CH_2)_n-$ chains], the geometry of the system is not well defined and it is difficult to rationalize the results obtained.

These problems are overcome by using rigid and modular spacers to connect the two chromophoric units; the systems so obtained have a well-characterized geometry and the energy transfer can occur over long distances. Interesting examples of this type of systems are the $[Ru(bpy)_3]^{2+}$–$(ph)_n$–$[Os(bpy)_3]^{2+}$ (ph = 1,4-phenylene; $n = 2$, 3, 4, 5) species [27] shown in Figure 1.7. In such compounds, excitation of the $[Ru(bpy)_3]^{2+}$ moiety is followed by energy transfer to the $[Os(bpy)_3]^{2+}$ unit, as shown by the sensitized emission of the latter (CH_3CN, 293 K). The energy-level diagram is shown schematically in Figure 1.7. The lowest energy level of the bridge decreases slightly as the number of phenylene units is increased, but always lies above the donor and acceptor levels involved in energy transfer. A further decrease in the energy of the triplet excited state of the spacer would be expected to switch the energy-transfer mechanism from superexchange-mediated to hopping, similar to what happens for photoinduced electron transfer. In the series of compounds shown in

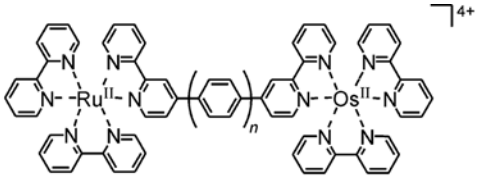

$n = 2$ $k_{en} = 2.5 \times 10^{11}\ s^{-1}$
$n = 3$ $k_{en} = 5.9 \times 10^{10}\ s^{-1}$
$n = 4$ $k_{en} = 4.1 \times 10^{9}\ s^{-1}$
$n = 5$ $k_{en} = 4.9 \times 10^{8}\ s^{-1}$

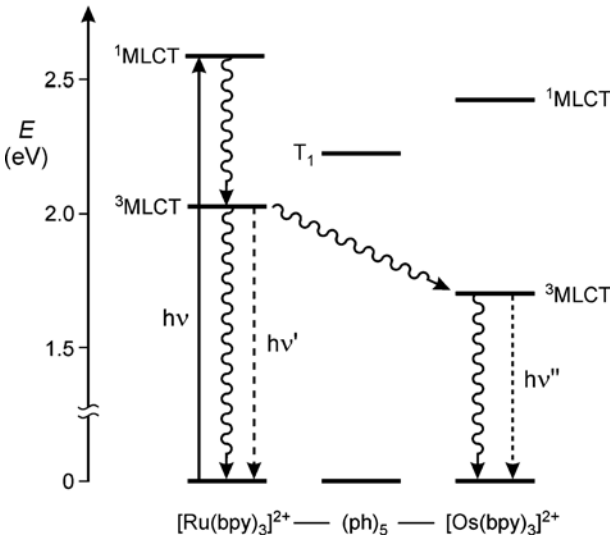

Figure 1.7 Structure of compounds $[Ru(bpy)_3]^{2+}$–$(ph)_n$–$[Os(bpy)_3]^{2+}$ and energy-level diagram for the energy-transfer process [27].

Figure 1.7, the energy-transfer rate decreases with increasing length of the oligophenylene spacer. Such rate constants are much higher than those expected for a Förster-type mechanism, whereas they can be accounted for by a superexchange Dexter mechanism [28]. The values obtained for energy transfer in the analogous series of compounds $[Ru(bpy)_3]^{2+}$–$(ph)_nR_2$–$[Os(bpy)_3]^{2+}$ [29], in which the central phenylene unit carries two hexyl chains, are much lower than those found for the unsubstituted compounds, most likely because the bulky substituents R increase the tilt angle between the phenyl units. A strong decrease in the rate constant is observed when the Ru-donor and Os-acceptor units are linked via an oligophenylene bridge connected in the meta position [30].

In an another family of similar compounds, $[Ir(ppyF_2)_2(bpy)]^{+}$–$(ph)_n$–$[Ru(bpy)_3]^{2+}$ (ph = 1,4-phenylene; $n = 2, 3, 4, 5$) [31], the energy-transfer rate constant is much higher and substantially independent of the length of the spacer. The energy-level

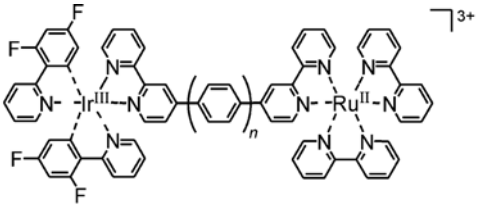

$n = 2$ $k_{en} = 8.3 \times 10^{11}\ s^{-1}$
$n = 3$ $k_{en} = 5.9 \times 10^{11}\ s^{-1}$
$n = 4$ $k_{en} = 3.6 \times 10^{11}\ s^{-1}$
$n = 5$ $k_{en} = 3.3 \times 10^{11}\ s^{-1}$

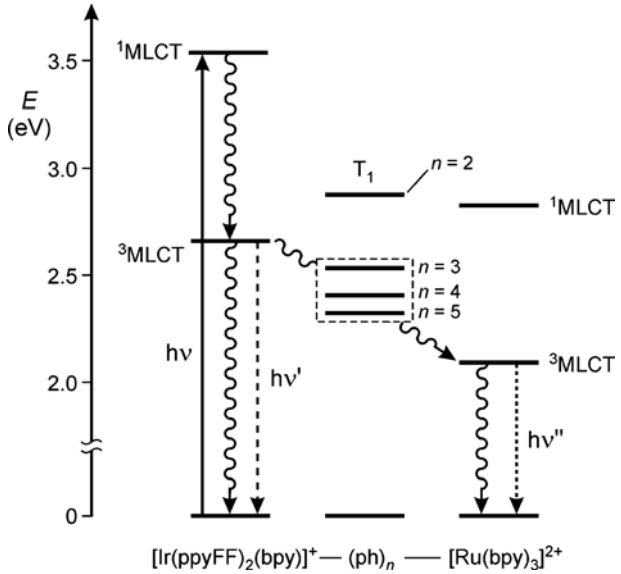

Figure 1.8 Structure of compounds $[Ir(ppyF_2)_2(bpy)]^{+}$–$(ph)_n$–$[Ru(bpy)_3]^{2+}$ and energy-level diagram for the energy-transfer process [31].

diagram for this family, displayed in Figure 1.8, shows that the energy level of the donor is almost isoenergetic with the triplet state of the spacers. The energy of the Ir-based donor can, therefore, be transferred to the Ru-based acceptor via hopping on the bridging ligand, at least for $n > 2$.

1.4
Switching Electron-Transfer Processes in Wire-Type Systems

A clever choice of molecular components and their assembly in suitable sequences allow the design of very interesting molecular-level photonic switches for photoinduced electron-transfer processes.

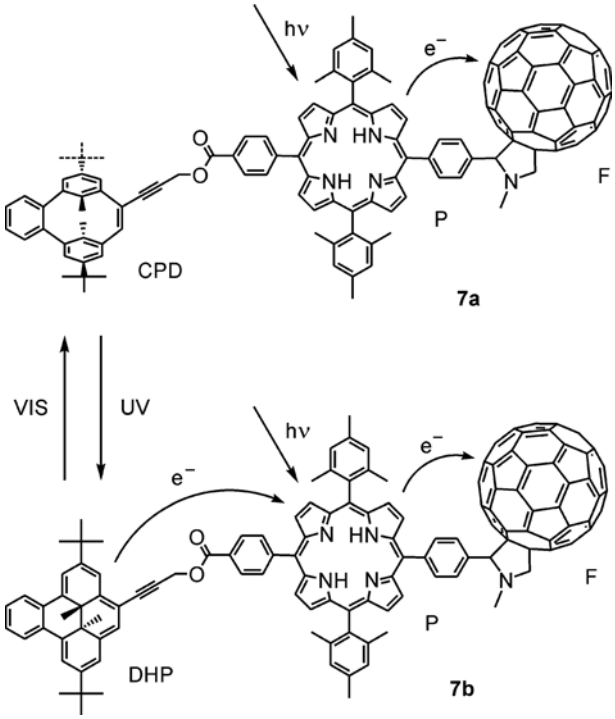

Figure 1.9 A single pole electron-transfer switch. Light-induced isomerization and electron transfer processes in triad **7** [32].

Triad **7** (Figure 1.9) is an example of electron transfer switch generated by the light-induced interconversion between the two forms of a chromophore. This triad, which performs as a single pole molecular switch, consists of a porphyrin unit (P) linked covalently to both a fullerene (F) electron acceptor and a dihydropyrene photochrome [32]. In structure **7a**, the photochrome is in the cyclophanediene (CPD) form, which absorbs light only in the UV region. Excitation of the porphyrin unit leads to $CPD-{}^1P-F$ excited state which undergoes electron transfer yielding the $CPD–P^+–F^-$ charge-separated state with unitary efficiency. Such a state then decays to the ground state with time constant 3.3 ns. Irradiation of **7a** with UV light at 254 nm converts the cyclophanediene form of the photochrome into the dihydropyrene form (DHP). The photochemistry of the resulting DHP–P–F species (**7b**) is different from that of **7a**. The $DHP-{}^1P-F$ excited state leads again to charge separation, $DHP–P^+–F^-$, but before the charge separated state can recombine to the ground state, an electron migrates from the DHP moiety to the porphyrin, producing $DHP^+–P–F^-$ with quantum yield 0.94. This state lives much longer (2.0 μs) than the $CPD–P^+–F^-$ species because the charges are much farther apart and, therefore, the electronic coupling is smaller. Reconfiguration of the system to **7a** can be obtained by visible light irradiation.

1.5
A Plug–Socket Device Based on a Pseudorotaxane

Supramolecular species whose components are connected by means of noncovalent forces can be disassembled and re-assembled [33] by modulating the interactions that keep the components together, with the consequent possibility of switching energy-transfer processes. Two-component systems of this type are reminiscent of plug–socket electrical devices because, like their macroscopic counterparts, they are characterized by (i) the possibility of connecting–disconnecting the two components in a reversible way and (ii) the occurrence of an electronic energy flow from the socket to the plug when the two components are connected (Figure 1.10a). Hydrogen-bonding interactions between ammonium ions and crown ethers are particularly

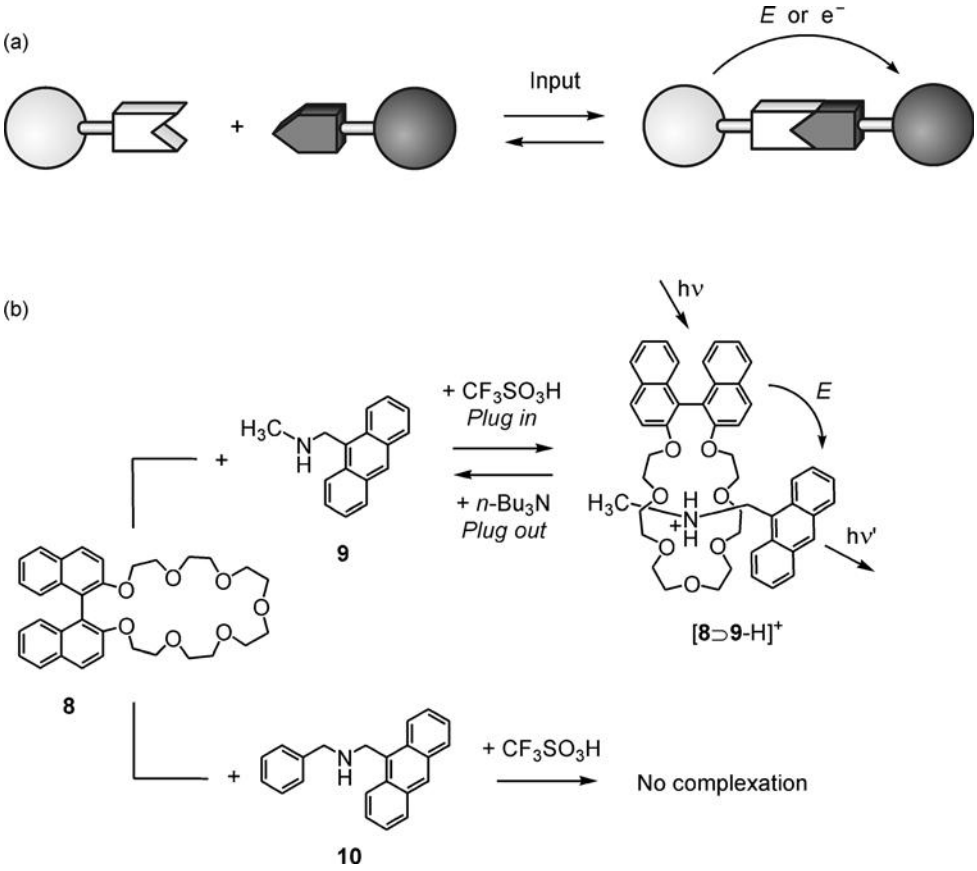

Figure 1.10 (a) Schematic representation of the working mechanism of a plug–socket system. (b) Switching of photoinduced energy transfer by the acid–base-controlled plug in–plug out of binaphthocrown ether **8** and anthracenylammonium ion **9**-H^+ [34].

suitable for constructing molecular-level plug–socket devices, since they can be switched on and off quickly and reversibly by means of acid–base inputs.

A plug–socket system which deals with the transfer of electronic energy is illustrated in Figure 1.10b [34]. The absorption and fluorescence spectra of a CH_2Cl_2 solution containing equal amounts of (±)-binaphthocrown ether **8** and amine **9** indicate the absence of any interaction between the two compounds. Addition of a stoichiometric amount of acid, capable of protonating **9**, causes profound changes in the fluorescence behavior of the solution, namely (i) the fluorescence of **8** is completely quenched and (ii) the fluorescence of **9**-H^+ is sensitized upon excitation with light absorbed exclusively by the crown ether. These observations are consistent with the formation of an adduct between **8** and **9**-H^+, wherein very efficient electronic energy transfer occurs from the photoexcited binaphthyl unit of the crown ether to the anthracenyl group incorporated within the **9**-H^+ component. Such an adduct belongs to the class of pseudorotaxanes, that is, supermolecules made (at the minimum) of a thread-like guest molecule surrounded by a macrocyclic host, because dialkylammonium ions are known [35] to penetrate the cavity of crown ethers such as **8**. The very fast rate constant ($k > 4 \times 10^9\ s^{-1}$) for the energy-transfer process [34] can be accounted for by a coulombic mechanism, as molecular models show that the maximum distance between binaphthyl and anthracene units in the **8** ⊃ **9**-H^+ complex (∼15 Å) is much shorter than their Förster radius (26 Å).

The pseudorotaxane **8** ⊃ **9**-H^+ can be disassembled by the subsequent addition of a stoichiometric amount of base, capable of deprotonating **9**-H^+, thereby interrupting the photoinduced energy flow, as indicated by the restoring of the initial absorption and fluorescence spectra. Moreover, the stability of this pseudorotaxane can be influenced by changing the nature of the counteranion of **9**-H^+ [36]. Interestingly, the plug-in process does not occur when a plug component incompatible with the size of the socket, such as the benzyl-substituted amine **10**, is employed (Figure 1.10b).

1.6 Mimicking Electrical Extension Cables at the Molecular Level

The plug–socket concept described above can be used to design molecular systems which mimic the function played by a macroscopic electrical extension cable. The operation of an extension cable is more complex than that of a plug–socket system, because it involves *three* components that must be held together by *two* connections that have to be controllable *reversibly* and *independently*; in the fully connected system, an electron or energy flow must take place between the remote donor and acceptor units (Figure 1.11).

In the attempt to construct a molecular-level extension cable for electron transfer, the pseudorotaxane shown in Figure 1.12a, made of the three components $\mathbf{11}^{2+}$, **12**-H^{3+} and **13**, has been obtained and studied [37]. Component $\mathbf{11}^{2+}$ consists of two moieties: an $[Ru(bpy)_3]^{2+}$ unit, which behaves as an electron donor under light excitation, and a dibenzo[24]crown-8 macrocycle, capable of playing the role of a hydrogen-bonding first socket. The dialkylammonium-based moiety of **12**-H^{3+},

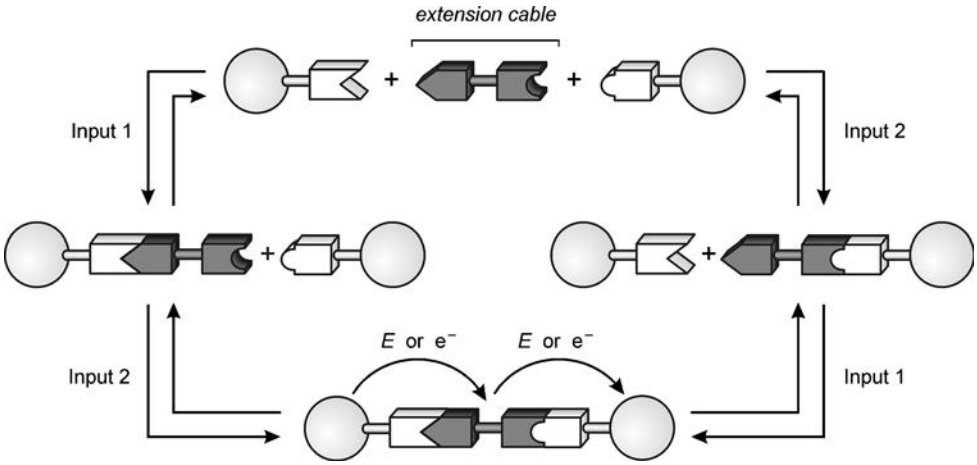

Figure 1.11 (a) Schematic representation of the working mechanism of an electrical extension cable.

driven by hydrogen-bonding interactions, threads as a plug into the first socket, whereas the π-electron accepting 4,4′-bipyridinium unit threads as a plug into the third component **13**, the π-electron rich 1,5-dinaphtho[38]crown-10 macrocycle, which plays the role of a second socket. In CH_2Cl_2–CH_3CN (98 : 2 v/v) solution, reversible connection–disconnection of the two plug–socket junctions can be controlled independently by acid–base and redox stimulation, respectively, and monitored by changes in the absorption and emission spectra, owing to the different nature of the interactions (hydrogen bonding and π-electron donor–acceptor) that connect the components. In the fully assembled triad, $\mathbf{11}^{2+} \supset \mathbf{12}\text{-}H^{3+} \subset \mathbf{13}$, light excitation of the $[Ru(bpy)_3]^{2+}$ unit of the component $\mathbf{11}^{2+}$ is followed by electron transfer to the bipyridinium unit of the component $\mathbf{12}\text{-}H^{3+}$, which is plugged into component **13**.

It should be noted that in the system described above, the transferred electron does not reach the final component of the assembly. Moreover, a true extension cable should contain a plug and a socket at the two ends, instead of two plugs as component $\mathbf{12}\text{-}H^{3+}$. An improved system of that type has been investigated recently (Figure 1.12**b**) [38]. The electron-source component is again $\mathbf{11}^{2+}$, whereas the new extension cable $\mathbf{14}\text{-}H^{+}$ is made up [39] of a dialkylammonium ion, that can insert itself as a plug into a dibenzo [24]crown-8 socket, a biphenyl spacer and a benzonaphtho [36] crown-10 unit, which fulfills the role of a π-electron-rich socket. Finally, the 1,1′-dioctyl-4,4′-bipyridinium dication $\mathbf{15}^{2+}$ can play the role of an electron drain plug. As for the previously studied system, the two plug–socket connections $\mathbf{11}^{2+} \supset \mathbf{14}\text{-}H^{+}$ and $\mathbf{14}\text{-}H^{+} \supset \mathbf{15}^{2+}$ can be controlled by acid–base and redox stimuli, respectively.

In the complete ensemble, $\mathbf{11}^{2+} \supset \mathbf{14}\text{-}H^{+} \supset \mathbf{15}^{2+}$, light excitation of the Ru-based unit of $\mathbf{11}^{2+}$ is followed by electron transfer to $\mathbf{15}^{2+}$, with $\mathbf{14}\text{-}H^{+}$ playing the role of an extension cable (Figure 1.12b). The occurrence of this process is confirmed by nanosecond laser flash photolysis experiments, showing a transient absorption

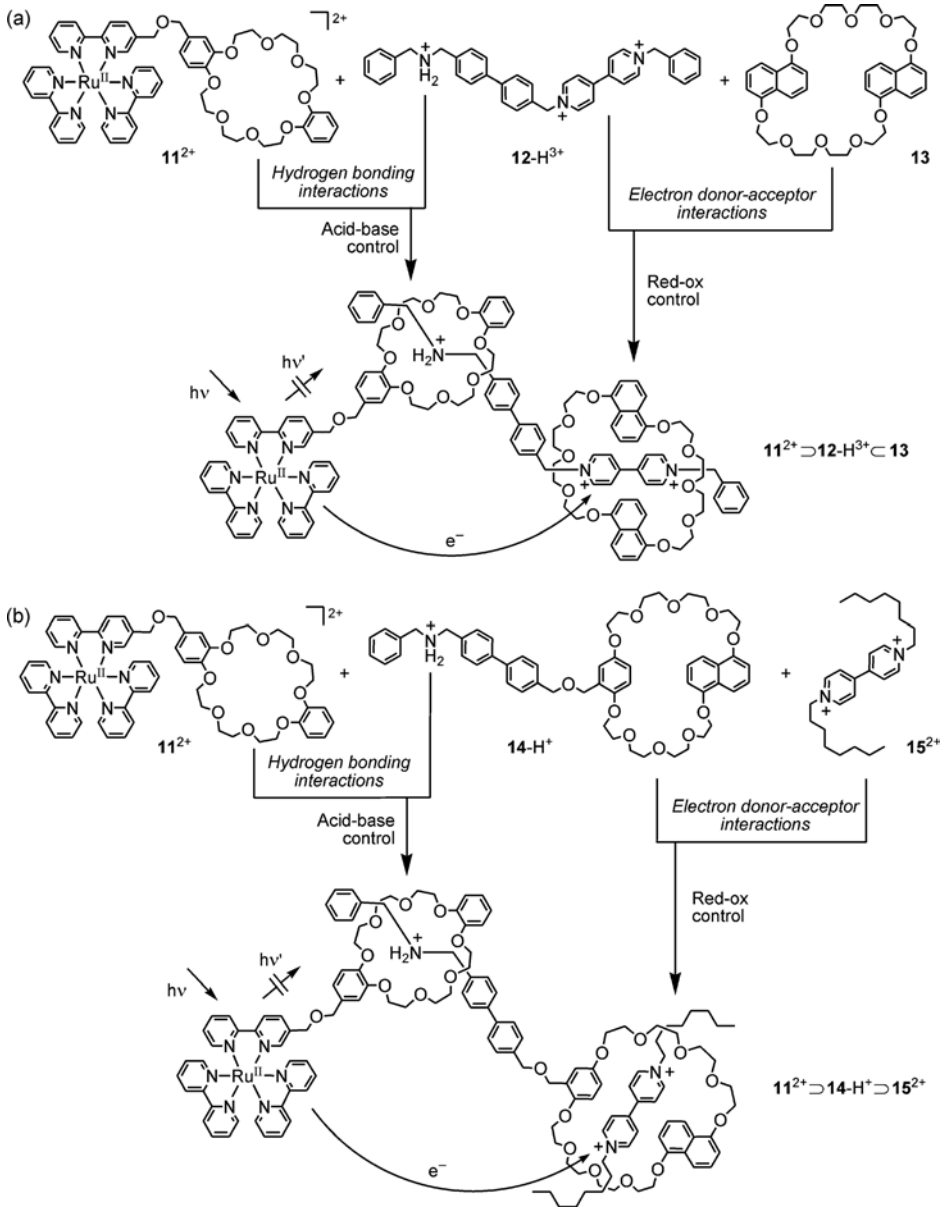

Figure 1.12 First- and second-generation systems for mimicking an electrical extension cable. (a) Structural formulas of the three molecular components $\mathbf{11}^{2+}$, $\mathbf{12}\text{-}H^{+}$ and **13**, which self-assemble in solution to give the $\mathbf{11}^{2+} \supset \mathbf{12}\text{-}H^{3+} \supset \mathbf{13}$ triad. The photoinduced electron-transfer process from the Ru-based unit of $\mathbf{11}^{2+}$ to the bipyridinium unit of $\mathbf{12}\text{-}H^{3+}$ taking place in the fully connected system is also represented [37]. (b) Structural formulas of the three molecular components $\mathbf{11}^{2+}$, $\mathbf{14}\text{-}H^{+}$ and $\mathbf{15}^{2+}$, which self-assemble in solution to give the $\mathbf{11}^{2+} \supset \mathbf{14}\text{-}H^{+} \supset \mathbf{15}^{2+}$ triad. In the fully connected system, excitation with visible light of the Ru-based unit of $\mathbf{11}^{2+}$ is followed by electron transfer to $\mathbf{15}^{2+}$, with $\mathbf{14}\text{-}H^{+}$ playing the role of an extension cable [38].

signal assigned to the 4,4′-bipyridinium radical cation formed by photoinduced electron transfer within the self-assembled triad. Such a second-generation system exhibits two conceptual and significant advancements: (i) **14**-H^+ consists of a plug and a socket components and thus it really mimics an extension cable; (ii) the photoinduced electron transfer does occur from the first component – the Ru-based unit of $\mathbf{11}^{2+}$ – to the remote $\mathbf{15}^{2+}$ moiety, whereas in the previous system the electron receiving bipyridinium unit was a component of the cable.

1.7 Light-Harvesting Antennas

An antenna for light harvesting (Figure 1.13) is an organized multicomponent system in which several chromophoric molecular species absorb the incident light and channel the excitation energy to a common acceptor component [40]. For artificial systems, the term "antenna effect" was first used [41] to discuss the case of strongly emitting but weakly absorbing lanthanide ions surrounded by strongly absorbing ligands, where the luminescence of the lanthanide ion was sensitized by excitation in the ligand-centered excited states. Research in this area is still very active [42]. Antenna systems are widely used by Nature to solve the problem of light-harvesting efficiency in the photosynthetic process where light is converted into chemical energy [43]. Collecting light by an antenna system, however, may also be useful for other purposes, such as signal amplification in luminescence sensors [44], photodynamic cancer therapy [45] and up-conversion processes [46]. A large system, where an array of chromophoric units absorb light and transfer energy to a luminescent center, can also be considered a spatial and spectral energy concentrator ("molecular lens") [47].

The antenna effect can only be obtained in supramolecular arrays suitably organized in the dimensions of time, energy and space. Each molecular component has to absorb the incident light and the excited state so obtained (donor) has to transfer electronic energy to a nearby component (acceptor), before undergoing radiative or nonradiative deactivation (organization in the time dimension). In order

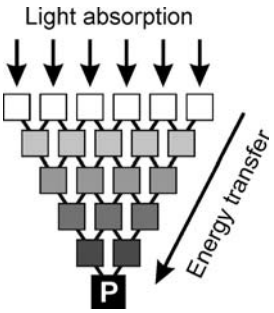

Figure 1.13 Schematic representation of a light-harvesting antenna system. Squares represent light-absorbing molecules. P is the molecule to which excitation energy is channeled. Excited state energy decreases with increasing shade.

for energy transfer to occur, the energy of the acceptor excited state has to be lower or, at most, equal to the energy of the excited state of the donor (organization in the energy dimension). Finally, the successive donor-to-acceptor energy-transfer steps must result in an overall energy-transfer process leading the excitation energy towards a selected component of the array (organization in the space dimension).

In the course of evolution, Nature has succeeded to build up antenna systems that fully satisfy the above requirements. In green plants, such natural antennae collect an enormous amount of solar energy and redirect it as electronic excitation energy to reaction centers where subsequent conversion into redox chemical energy takes place. In recent years, the development of supramolecular chemistry (particularly of dendrimer chemistry) and the high level of experimental and theoretical efficacy reached by photochemistry have enabled scientists to design and construct a number of interesting artificial antenna systems.

Dendrimer $\mathbf{16}^{2+}$ (Figure 1.14) is a classical example of antenna system [48]. The 2,2′-bipyridine ligands of the $[Ru(bpy)_3]^{2+}$-type [49] core carry branches containing

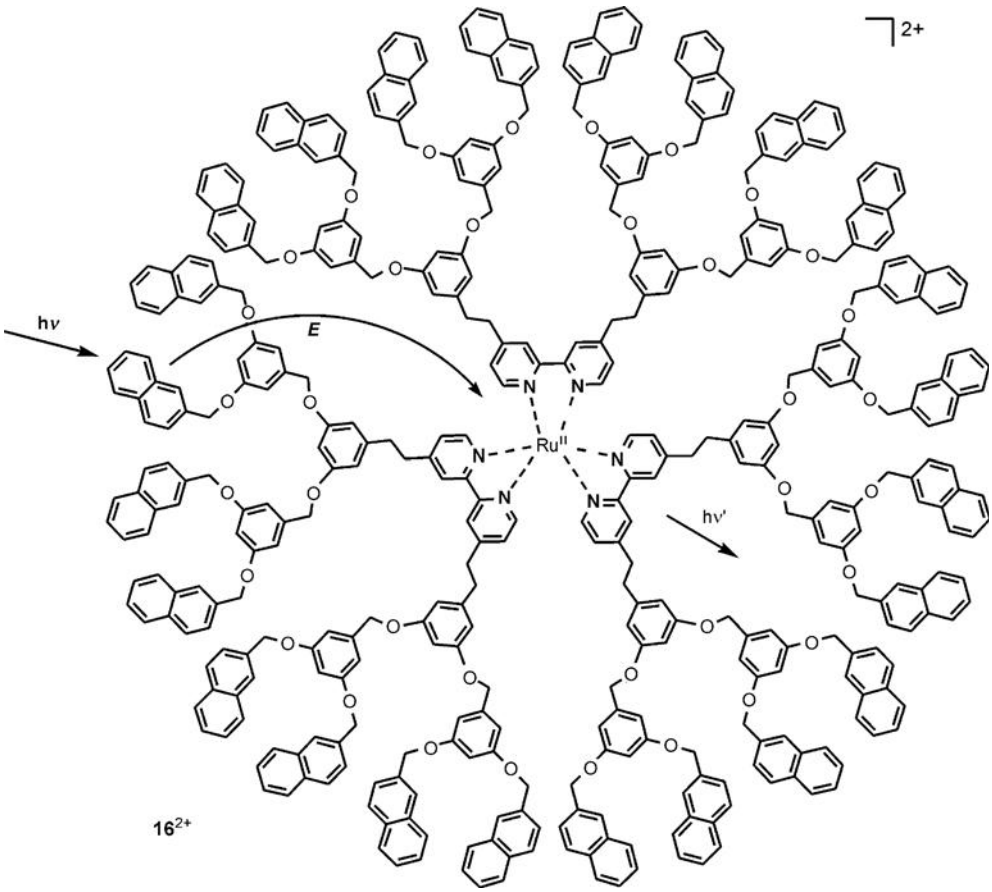

Figure 1.14 Antenna effect in dendrimer $\mathbf{16}^{2+}$ with $[Ru(bpy)_3]^{2+}$ core [48].

1,2-dimethoxybenzene- and 2-naphthyl-type chromophoric units. Because such units (as well as the core) are separated by aliphatic connections, the interchromophoric interactions are weak and the absorption spectrum of the dendrimer is substantially equal to the summation of the spectra of the chromophoric groups that are present in its structures. The three types of chromophoric groups, namely, $[Ru(bpy)_3]^{2+}$, dimethoxybenzene and naphthalene, are potentially luminescent species. In the dendrimer, however, the fluorescence of the dimethoxybenzene- and naphthyl-type units is almost completely quenched in acetonitrile solution, with concomitant sensitization of the luminescence of the $[Ru(bpy)_3]^{2+}$ core ($\lambda_{max} = 610$ nm). These results show that a very efficient energy-transfer process takes place converting the very short-lived (nanosecond time-scale) UV fluorescence of the aromatic units of the wedges to the long-lived (microsecond time-scale) orange emission of the metal-based dendritic core. It should also be noted that in aerated solution the luminescence intensity of the dendrimer core is more than twice as intense as that of the $[Ru(bpy)_3]^{2+}$ parent compound because the dendrimer branches protect the Ru-bpy based core from dioxygen quenching [50]. In conclusion, because of the very high absorbance of the naphthyl groups in the UV spectral region, the high energy-transfer efficiency and the strong emission of the $[Ru(bpy)_3]^{2+}$-type core, dendrimer $\mathbf{16}^{2+}$ (Figure 1.14) exhibits a strong visible emission upon UV excitation even in very dilute (10^{-7} mol L^{-1}) solutions [48].

1.8
Artificial Molecular Machines

1.8.1
Introduction

Natural molecular-level machines and motors are extremely complex systems. Any attempt to construct systems of such complexity by using an artificial bottom-up molecular approach would be hopeless. In the field of artificial systems, we can only construct simple prototypes consisting of a few molecular components, but we can use a chemical toolbox much larger than that used by Nature, exploit innovative ideas and operate in a much wider range of conditions (particularly as far as energy supply is concerned).

It designing artificial molecular devices, it should be recalled that they cannot be "shrunk" versions of macroscopic counterparts, because the operational mechanisms of motion at the molecular level have to deal with phenomena different from those that govern the macroscopic world [51,52]. Gravity and inertia motions that we are familiar with in our everyday experience are negligible at the molecular scale, where the viscous forces resulting from intermolecular interactions (including those with solvent molecules) largely prevail. This means that although we can describe the bottom-up construction of a nanoscale device as an assembly of suitable (molecular) components by analogy with what happens in the macroscopic world, we should not forget that the design principles and the operating mechanisms at the molecular level are different.

Mechanical movements at the molecular level result from nuclear motions caused by chemical reactions. Any kind of chemical reaction involves, of course, some nuclear displacement, but only large-amplitude, nontrivial motions leading to real translocation of some component parts of the system are considered. Particularly interesting nuclear motions from the viewpoint of artificial molecular systems are those related to (i) isomerization reactions involving −N=N−, −C=N− and −C=C− double bonds in covalent supramolecular structures, (ii) acid–base or redox reactions causing making or breaking of intermolecular bonds (including hydrogen bonds) and (iii) metal–ligand reactions causing the formation or disruption of coordination bonds.

Like macroscopic systems, mechanical molecular-level systems are characterized by: (a) the kind of energy supplied to make them work; (b) the kind of movement performed by their components; (c) the way in which their operation can be controlled and monitored; (d) the possibility of repeating the operation at will; (e) the time-scale needed to complete a cycle of operation; and (f) the function performed. Particularly interesting is the way in which energy can be supplied.

1.8.2 Energy Supply

To make a molecular machine move, energy must be supplied. The most obvious way of supplying energy to a chemical system is by adding a reactant (fuel) capable of causing a desired reaction. In his famous address "There is Plenty of Room at the Bottom" to the American Physical Society, R.P. Feynman discussed the possibility of constructing molecular-level machines and observed [53]: "*An internal combustion engine of molecular size is impossible. Other chemical reactions, liberating energy when cold, can be used instead*". This is exactly what happens in our body, in which the chemical energy, ultimately derived from food and oxygen, is used in a long series of slightly exoergonic reactions to power the biological machines that sustain life.

If an artificial molecular-level machine must work by inputs of chemical energy, it will need addition of fresh reactants ("fuel") at any step of its working cycle [54]. It should be noticed that even cycling between two forms of a molecular-level system under the action of chemical inputs implies formation of waste products. For example, if the forward reaction is caused by an acid input, successive addition of a base will return the system to its original form, but the acid–base reaction generates waste products. Accumulation of waste products will inevitably compromise the operation of the machine, unless they are removed from the system, as happens both in natural machines and in macroscopic internal combustion engines.

The need to remove waste products introduces noticeable limitations in the design and construction of artificial molecular machines and motors based on "chemical fuel" inputs [55]. All the proposed systems operating by use of chemical energy become increasingly less efficient on increasing the number of cycles and finally stop working.

There are, however, alternative, more convenient, ways of powering artificial molecular machines.

1.8.3 Light Energy

In green plants the energy needed to sustain the machinery of life is provided by sunlight [43]; in general, light energy is not used as such to produce mechanical movements, but it is used to produce a chemical fuel, namely ATP, suitable for feeding natural molecular machines. Light energy, however, can directly cause photochemical reactions involving large nuclear movements. A simple example is a photoinduced isomerization from the lower energy *trans* to the higher energy *cis* form of a molecule containing −C=C− or −N=N− double bonds; this is followed by a spontaneous or light-induced back reaction [9,10]. Such photoisomerization reactions have indeed been used to make molecular machines driven by light energy inputs [56]. In supramolecular species, photoinduced electron-transfer reactions can often cause large displacement of molecular components [6,7,10,57]. Indeed, working with suitable systems, an endless sequence of cyclic molecular-level movements can in principle be performed making use of light-energy inputs without generating waste products [55,58].

Compared with chemical energy inputs, photonic energy has other advantages, besides the fundamental one of not generating waste products: (i) light can be switched on/off easily and rapidly; (ii) lasers provide the opportunity of working in very small space and very short time domains; (iii) photons, besides supplying the energy needed to make a machine work, can also be useful to "read" the state of the system and thus to control and monitor the operation of the machine. For all these reasons, photonic energy is extensively used to power artificial molecular machines.

Here we will briefly describe two examples: the first is based on a photoisomerization reaction, whereas the second relies on photoinduced electron-transfer processes.

1.8.4 Threading–Dethreading of an Azobenzene-Based Pseudorotaxane

Pseudorotaxanes are interesting in the context of molecular machinery, because the assembly–disassembly of the thread-like and macrocyclic components reminds one of the threading–dethreading of a needle. They can hardly be used to make unimolecular machines because of the chemical equilibrium between the components, but they represent good models for the development of rotaxane- and catenane-based systems.

An example of a pseudorotaxane exhibiting threading–dethreading motions based on a photoisomerization process is shown in Figure 1.15 [59]. The thread-like species *trans*-**17**, which contains a π-electron rich azobiphenoxy unit, and the π-electron-deficient macrocycle $\mathbf{18}^{4+}$ self-assemble very efficiently to give a

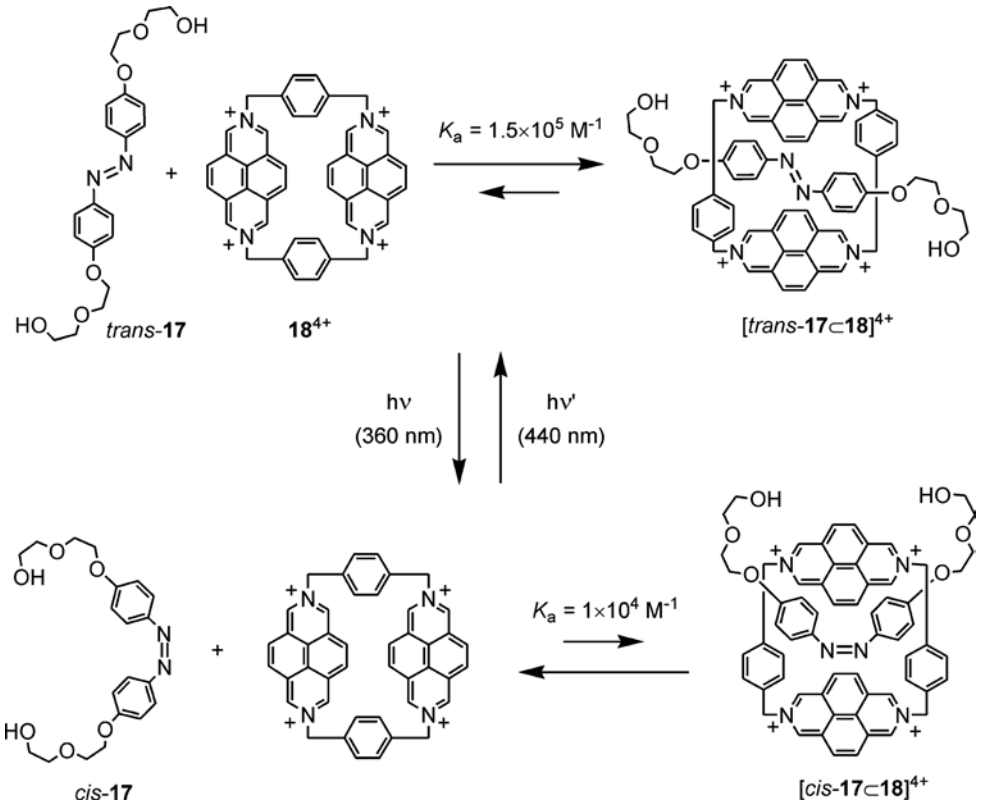

Figure 1.15 Threading–dethreading of **17** and $\mathbf{18}^{4+}$ as a consequence of the *cis–trans* photoisomerization of the azobenzene-type unit contained in the thread-like component **17** [48].

pseudorotaxane, stabilized by electron donor–acceptor interactions. The association constant, obtained by fluorescence titration in acetonitrile solution at room temperature, is $K_a = (1.5 \pm 0.2) \times 10^5\,\mathrm{L\,mol^{-1}}$. In the pseudorotaxane structure, the intense fluorescence characteristic of free $\mathbf{18}^{4+}$ ($\lambda_{max} = 434$ nm, Figure 1.16) is completely quenched by the donor–acceptor interaction.

Irradiation of an acetonitrile solution containing $1.0 \times 10^{-4}\,\mathrm{mol\,L^{-1}}$ *trans*-**17** and $\mathbf{18}^{4+}$ (ca. 80% complexed species) with 365-nm light – almost exclusively absorbed by the *trans*-azobiphenoxy unit – causes strong absorption spectral changes, as expected for the well-known *trans* → *cis* photoisomerization of the azobenzene-type moiety. Such spectral changes are accompanied by a parallel increase in the intensity of the fluorescence band with $\lambda_{max} = 434$ nm (Figure 1.16), characteristic of free $\mathbf{18}^{4+}$ (see above). This behavior shows that photoisomerization is accompanied by dethreading (Figure 1.15), a result which is confirmed by the finding that the association constant of $\mathbf{18}^{4+}$ with *cis*-**17**, $K_a = (1.0 \pm 0.1) \times 10^4\,\mathrm{L\,mol^{-1}}$, is much smaller than that with

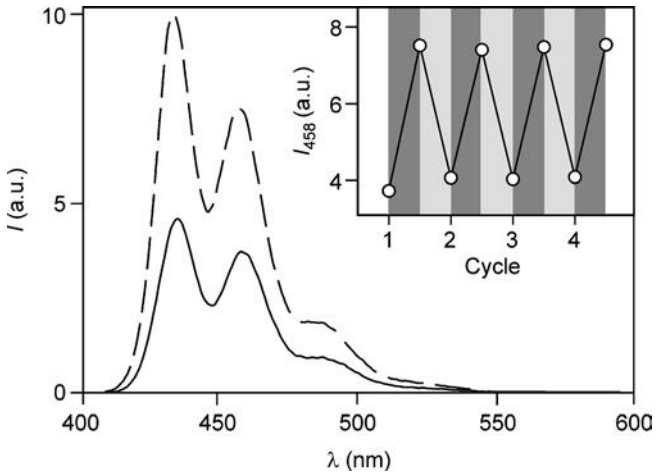

Figure 1.16 Fluorescence spectrum of an equimolar mixture (1.0×10^{-4} mol L^{-1}) of *trans*-**17** and $\mathbf{18}^{4+}$ in acetonitrile at room temperature (full line) and fluorescence spectrum of the same mixture after irradiation at 365 nm until a photostationary state is reached (dashed line). The inset shows the changes in intensity of the fluorescence associated with the free macrocyclic ring $\mathbf{18}^{4+}$ upon consecutive *trans* → *cis* (irradiation at 365 nm, dark areas) and *cis trans* → *cis trans* (irradiation at 436 nm, light areas) photoisomerization cycles. Excitation is performed in an isosbestic point at 411 nm [59].

trans-**17**. On irradiation at 436 nm or by warming the solution in the dark, the *trans* isomer of **17** can be reformed. This process is accompanied by a parallel decrease in the fluorescence intensity at $\lambda_{max} = 434$ nm, indicating that the *trans*-**17** species rethreads through the macrocycle $\mathbf{18}^{4+}$.

Although this system is a rudimentary attempt towards the making of light-driven molecular machines, it should be noted that it exhibits a number of valuable features. First, threading-dethreading is controlled exclusively by light energy, without generation of waste products. Furthermore, owing to the reversibility of the photoisomerization process, the light-driven dethreading–rethreading cycle can be repeated at will (Figure 1.16, inset). Another relevant feature of this system is that it exhibits profound changes of a strong fluorescence signal.

1.8.5
Photoinduced Shuttling in Multicomponent Rotaxanes: a Light-Powered Nanomachine

Rotaxanes are appealing systems for the construction of molecular machines because the mechanical binding of the macrocyclic host with its dumbbell-shaped substrate leaves the former free to displace itself along and/or around the latter without losing the system's integrity. Two interesting molecular motions can be envisaged in rotaxanes, namely (i) rotation of the macrocyclic ring around the thread-like portion of the dumbbell-shaped component and (ii) translation of the ring along the same portion. The molecular components of a rotaxane usually exhibit some kind of

interaction originating from complementary chemical properties, which is also exploited in the template-directed synthesis of such systems. In rotaxanes containing two different recognition sites in their thread-like portion, it is possible to switch the position of the ring between these two "stations" by an external stimulus. Systems of this type, termed molecular shuttles [60], probably constitute the most common examples of artificial molecular machines. Interestingly, the dumbbell component of a molecular shuttle exerts a restriction on the ring motion in the three dimensions of space, similar to that imposed by the protein track for linear biomolecular motors kinesin and dynein [61].

On the basis of the experience gained with pseudorotaxane model systems [62], the rotaxane $\mathbf{19}^{6+}$ (Figure 1.17) was specifically designed [63] to achieve photoinduced ring shuttling in solution. This compound has a modular structure; its ring component R is a π-electron-donating bis-*p*-phenylene [34]crown-10, whereas its dumbbell component is made of several covalently linked units. They are a Ru(II)-polypyridine complex (P^{2+}), a *p*-terphenyl-type rigid spacer (S), a 4,4′-bipyridinium (A_1^{2+}) and a 3,3′-dimethyl-4,4′-bipyridinium (A_2^{2+}) π-electron-accepting stations and a

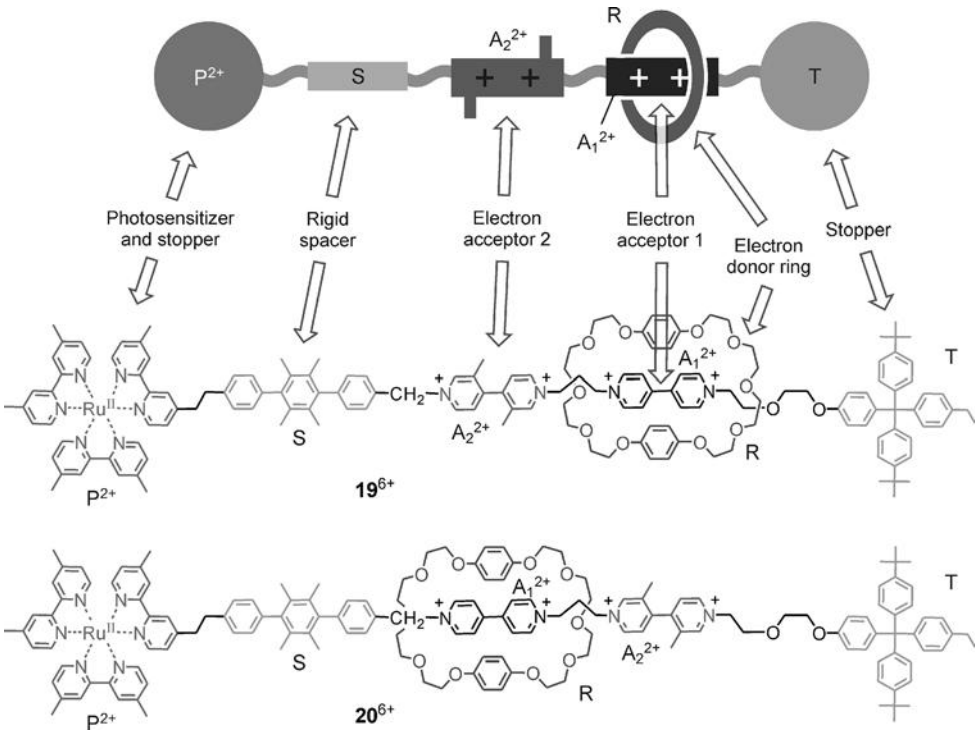

Figure 1.17 Structural formulas of multicomponent rotaxanes $\mathbf{19}^{6+}$ [63] and $\mathbf{20}^{6+}$ [66], designed to work as photochemically driven molecular shuttles. A cartoon representation of $\mathbf{19}^{6+}$ is also shown.

tetraarylmethane group as the terminal stopper (T). The Ru-based unit plays the dual role of a light-fueled power station and a stopper, whereas the mechanical switch consists of the two electron-accepting stations and the electron-donating macrocycle. The stable translational isomer of rotaxane $\mathbf{19}^{6+}$ is the one in which the R component encircles the A_1^{2+} unit, in keeping with the fact that this station is a better electron acceptor than the other.

The strategy devised in order to obtain the photoinduced shuttling movement of the macrocycle between the two stations A_1^{2+} and A_2^{2+} is based on the following "four-stroke" synchronized sequence of electronic and nuclear processes (Figure 1.18):

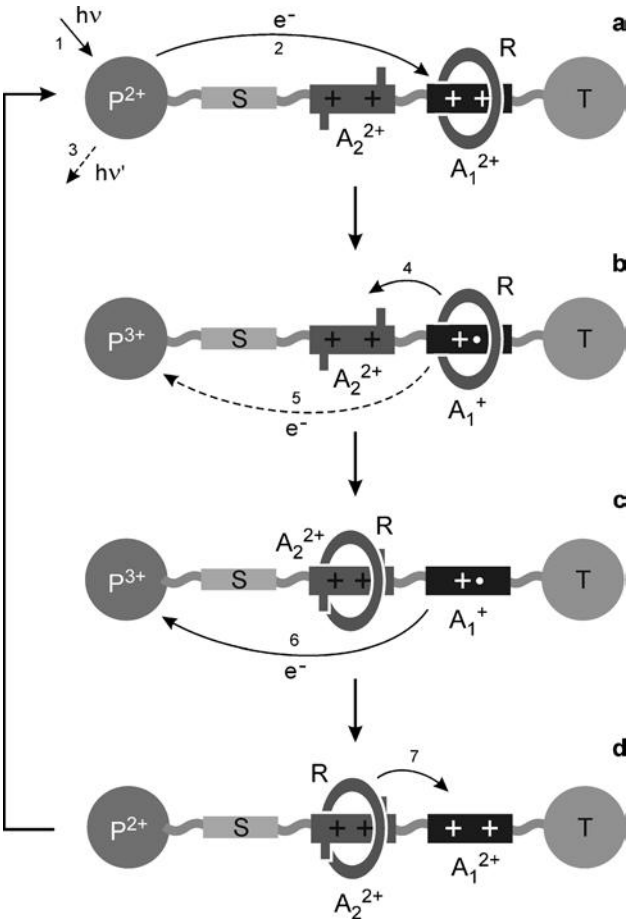

Figure 1.18 Schematic representation of the working mechanism of rotaxane $\mathbf{19}^{6+}$ as an autonomous "four-stroke" molecular shuttle powered by visible light [64]. See Figure 1.17 for the legend for the cartoons.

(a) *Destabilization of the stable translational isomer:* light excitation of the photoactive unit P^{2+} (process *1*) is followed by the transfer of an electron from the excited state to the A_1^{2+} station, which is encircled by the ring R (process *2*), with the consequent "deactivation" of this station; such a photoinduced electron-transfer process competes with the intrinsic decay of the P^{2+} excited state (process *3*).

(b) *Ring displacement:* the ring moves (process *4*) for 1.3 nm from the reduced station A_1^{+} to A_2^{2+}, a step that is in competition with the back electron-transfer process from A_1^{+} (still encircled by R) to the oxidized unit P^{3+} (process *5*).

(c) *Electronic reset:* a back electron-transfer process from the "free" reduced station A_1^{+} to the oxidized unit P^{3+} (process *6*) restores the electron acceptor power to such a station. At this point the machine is reset and the ring has been "pumped" into an energetically higher state.

(d) *Nuclear reset:* as a consequence of the electronic reset, thermally activated back movement of the ring from A_2^{2+} to A_1^{2+} takes place (process *7*).

Steady-state and time-resolved spectroscopic experiments together with electrochemical measurements in acetonitrile solution showed [64] that the absorption of a visible photon by $\mathbf{19}^{6+}$ can cause the occurrence of a forward and back ring movement, that is, a full mechanical cycle according to the mechanism illustrated in Figure 1.18 [65]. It was estimated that the fraction of the excited-state energy used for the motion of the ring amounts to ~10% and the system can generate a mechanical power of about 3×10^{-17} W per molecule. The somewhat disappointing quantum efficiency for ring shuttling (2% at 30 °C) is compensated for by the fact that the investigated system gathers together the following features: (i) it is powered by visible light (in other words, sunlight); (ii) it exhibits autonomous behavior, like motor proteins; (iii) it does not generate waste products; (iv) its operation can rely only on intramolecular processes, allowing in principle operation at the single-molecule level; (v) it can be driven at a frequency of about 1 kHz; (vi) it works in mild environmental conditions (i.e. fluid solution at ambient temperature); and (vii) it is stable for at least 10^3 cycles.

The molecular shuttle $\mathbf{19}^{6+}$ can also be operated, with a higher quantum yield, by a sacrificial mechanism [63] based on the participation of external reducing (triethanolamine) and oxidizing (dioxygen) species and by an intermolecular mechanism [64] involving the kinetic assistance of an external electron relay (phenothiazine), which is not consumed. However, operation by the sacrificial mechanism does not afford an autonomous behavior and leads to consumption of chemical fuels and formation of waste products. On the other hand, the assistance by an electron relay affords autonomous operation in which only photons are consumed, but the mechanism is no longer based solely on intra-rotaxane processes.

Owing to its modular design, the rotaxane $\mathbf{19}^{6+}$ is amenable to structural modification in an attempt to improve its performance as a light-driven molecular shuttle. For instance, the rotaxane $\mathbf{20}^{6+}$ (Figure 1.17), which differs from $\mathbf{19}^{6+}$ only in the exchange of the position of the two electron-accepting stations along the dumbbell-shaped component, has been recently synthesized and its photochemical

properties investigated [66]. It has been found that the shorter distance of the electron-transfer photosensitizer P^{2+} to the better (A_1^{2+}) of the two electron acceptors in $\mathbf{20}^{6+}$ results in an increase in the rate – and hence the efficiency – of the photoinduced electron-transfer step compared with $\mathbf{19}^{6+}$. The rate of the back electron transfer, however, also increases. As a consequence, such a second-generation molecular shuttle performs better than $\mathbf{19}^{6+}$ in a sacrificial mechanism, but much worse when it is powered by visible light (e.g. sunlight) alone. Another interesting difference between these two parent rotaxanes lies in the fact that the macrocyclic ring R, which initially surrounds the A_1^{2+} station, moves in opposite directions upon light excitation, i.e. towards the photosensitizer P^{2+} in $\mathbf{19}^{6+}$ and towards the stopper T in $\mathbf{20}^{6+}$.

This study shows that the structural and functional integration of different molecular subunits in a multicomponent structure is a powerful strategy for constructing nanoscale machines [67]. Nevertheless, the molecular shuttle $\mathbf{19}^{6+}$ in its present form could not perform a net mechanical work in a full cycle of operation [68] (as for any reversible molecular shuttle, the work done in the "forward" stroke would be cancelled by the "backward" stroke) [69]. To reach this goal, a more advanced design of the molecular machine and/or a better engineering of its operating environment (e.g. a surface or a membrane) are required [6].

1.9 Conclusion

One of the most interesting aspects of supramolecular (multicomponent) systems is their interaction with light. The systems described here show that, in the frame of research on supramolecular photochemistry, the design and construction of nanoscale devices capable of performing useful light-induced functions can indeed be attempted.

The potential applications of photochemical molecular devices and machines are various – from energy conversion to sensoring and catalysis – and, to a large extent, still unpredictable. As research in the area is progressing, two interesting kinds of unconventional applications of these systems begin to emerge: (i) their behavior can be exploited for processing information at the molecular level [70] and, in the long run, for the construction of chemical computers [71]; and (ii) their mechanical features can be utilized for transportation of nano-objects, mechanical gating of molecular-level channels and nanorobotics [72].

However, it should be noted that the species described here, as most multicomponent systems developed so far, operate in solution, that is, in an incoherent fashion and without control of spatial positioning. Although the solution studies are of fundamental importance to understand their operation mechanisms and for some use (e.g. drug delivery), it seems reasonable that before such systems can find applications in many fields of technology, they will have to be interfaced with the macroscopic world by ordering them in some way. The next generation of multicomponent molecular species will need to be organized so that they can behave

coherently and can be addressed in space. Viable possibilities include deposition on surfaces, incorporation into polymers, organization at interfaces or immobilization into membranes or porous materials. Recent achievements in this direction [73–76] suggest that useful devices based on functional (supra)molecular systems could be obtained in the not too distant future.

Apart from foreseeable applications related to the development of nanotechnology, investigations on photochemical molecular devices and machines are important to increase the basic understanding of photoinduced reactions and other important processes such as self-assembly, and also to develop reliable theoretical models. This research also has the important merit of stimulating the ingenuity of chemists, thereby instilling new life into chemistry as a scientific discipline.

Acknowledgments

Financial support from the European Union (STREP "Biomach" NMP2-CT-2003–505487), MIUR (PRIN 2006034123-001), Regione Emilia-Romagna (NANO-FABER) and the University of Bologna is gratefully acknowledged.

References

1 Hader, D.-P. and Tevini, M. (1987) *General Photobiology*, Pergamon Press, Oxford.

2 Nalwa, H.S. (ed.) (2003) *Handbook of Photochemistry and Photobiology*, American Scientific Publishers, Stevenson Ranch, CA, vols. 1–4.

3 Joachim, C. and Launay, J.P. (1984) *Nouv. J. Chem.*, **8**, 723.

4 Balzani, V., Moggi, L. and Scandola, F. (1987) *Supramolecular Photochemistry* (ed. V. Balzani), Reidel, Dordrecht, p. 1.

5 Lehn, J.-M. (1988) *Angew. Chem. Int. Ed.*, **27**, 89.

6 Balzani, V., Credi, A. and Venturi, M. (2003) *Molecular Devices and Machines – a Journey into the Nano World*, Wiley-VCH, Weinheim.

7 Balzani, V., Credi, A., Raymo, F.M. and Stoddart, J.F. (2000) *Angew. Chem. Int. Ed.*, **39**, 3348.

8 Kay, E.R., Leigh, D.A. and Zerbetto, F. (2007) *Angew. Chem. Int. Ed.*, **46**, 72.

9 Gilbert, A. and Baggott, J. (1991) *Essentials of Molecular Photochemistry*, Blackwell Science, London.

10 Balzani, V. and Scandola, F. (1991) *Supramolecular Photochemistry*, Ellis Horwood, Chichester.

11 Balzani, V. (ed.) (2001) *Electron Transfer in Chemistry*, Wiley-VCH, Weinheim, vols. 1–5.

12 Nalwa, H.S. (ed.) (2003) *Handbook of Photochemistry and Photobiology*, American Scientific Publishers, Stevenson Ranch, CA, vols. 1–4.

13 Michl, J. (2006) in *Handbook of Photochemistry*, 3rd edn (eds M. Montalti, A. Credi, L. Prodi and M.T. Gandolfi) CCR, Taylor and Francis, New York. p. 1.

14 Balzani, V. (2006) in *Handbook of Photochemistry* 3rd edn (eds M. Montalti, A. Credi, L. Prodi and M.T. Gandolfi) CCR, Taylor and Francis, New York, p. 49.

15 Lakowicz, J.R. (2006) *Principles of Fluorescence Spectroscopy*, 3rd edn Springer, Singapore.

16 Montalti M., Credi A., Prodi L. and Gandolfi M.T. (eds) (2006) *Handbook of Photochemistry*, 3rd edn CCR, Taylor and Francis, New York.

17 Balzani, V., Bolletta, F., Gandolfi, M.T. and Maestri, M. (1978) *Top. Curr. Chem.*, **75**, 1.

18 *Adv. Chem. Phys.* (1999). pp. 106–107 special volumes (eds M. Bixon, J. Jortner) on Electron Transfer: from Isolated Molecules to Biomolecules.

19 May, V. and Kühn, O. (2000) *Charge and Energy Transfer Dynamics in Molecular Systems*, Wiley-VCH, Weinheim.

20 Gray, H.B. and Winkler, J.R. (2003) *Q. Rev. Biophys.*, **36**, 341.

21 Indelli, M.T., Bignozzi, C.A., Harriman, A., Schoonover, J.R. and Scandola, F. (1994) *J. Am. Chem. Soc.*, **116**, 3768.

22 Indelli, M.T., Chiorboli, C., Flamigni, L., De Cola, L. and Scandola, F. (2007) *Inorg. Chem*, **46**, 5630.

23 Juris, A., Balzani, V., Barigelletti, F., Campagna, S., Belser, P. and von Zelewsky, A. (1988) *Coord. Chem. Rev.*, **84**, 85.

24 Balzani, V. and Scandola, F. (1996) *Comprehensive Supramolecular Chemistry* (eds J.L. Atwood, J.E.D. Davies, D.D. MacNicol and F. Vögtle), Pergamon Press, Oxford, vol. 10, p. 687.

25 Flamigni, L., Baranoff, E., Collin, J.-P. and Sauvage, J.-P. (2006) *Chem. Eur. J.*, **12**, 6592.

26 Th. Förster, *Discuss. Faraday Soc.*, **1959**, *27*, 7. Note that in this paper there is a misprint since in Eq. (29) π^6 is used instead of π^5. See (a) Förster, Th. (1965) *Modern Quantum Chemistry* (ed. O. Sinanoğlu) Academic Press New York Part III: Action of Light and Organic Crystals,93. (b) Barigelletti, F. and Flamigni, L. (2000) *Chem. Soc. Rev.*, **29**, 1. (c) Scholes, G.D. (2003) *Annu. Rev. Phys. Chem.*, **54**, 57.

27 Welter, S., Salluce, N., Belser, P., Groeneveld, M. and De Cola, L. (2005) *Coord. Chem. Rev.*, **249**, 1360.

28 Dexter, D.L. (1953) *J. Chem. Phys.*, **21**, 836.

29 Schlicke, B., Belser, P., De Cola, L., Sabbioni, E. and Balzani, V. (1999) *J. Am. Chem. Soc.*, **121**, 4207.

30 D'Aleo, A., Welter, S., Cecchetto, E. and De Cola, L. (2005) *Pure Appl. Chem.*, **77**.1035.

31 Welter, S., Lafolet, F., Cecchetto, E., Vergeer, F. and De Cola, L. (2005) *ChemPhysChem*, **6**, 2417.

32 Liddell, P.A., Kodis, G., Andréasson, J., de la Garza, L., Bandyopadhyay, S., Mitchell, R.H., Moore, T.A., Moore, A.L. and Gust, D. (2004) *J. Am. Chem. Soc.*, **126**, 4803.

33 Balzani, V., Credi, A. and Venturi, M. (2002) *Proc. Natl. Acad. Sci. USA*, **99**, 4814.

34 Ishow, E., Credi, A., Balzani, V., Spadola, F. and Mandolini, L. (1999) *Chem. Eur. J.*, **5**, 984.

35 (a) Kolchinski, A.G., Busch, D.H. and Alcock, N.W. (1995) *J. Chem. Soc., Chem. Commun.*, 1289. (b) Ashton, P.R., Campbell, P.J., Chrystal, E.J.T., Glink, P.T., Menzer, S., Philp, D., Spencer, N., Stoddart, J.F., Tasker, P.A. and Williams, D.J. 1865 *Angew. Chem. Int. Ed.*, **1995**, **34**,

36 Clemente-León, M., Pasquini, C., Hebbe-Viton, V., Lacour, J., Dalla Cort, A. and Credi, A. (2006) *Eur. J. Org. Chem.*, 105.

37 Ballardini, R., Balzani, V., Clemente-Leon, M., Credi, A., Gandolfi, M.T., Ishow, E., Perkins, J., Stoddart, J.F., Tseng, H.-R. and Wenger, S. (2002) *J. Am. Chem. Soc.*, **124**, 12786.

38 Ferrer, B., Rogez, G., Credi, A., Ballardini, R., Gandolfi, M.T., Balzani, V., Liu, Y., Tseng, H.-R. and Stoddart, J.F. (2006) *Proc. Natl. Acad. Sci. USA*, **103**, 18411.

39 Rogez, G., Ferrer Ribera, B., Credi, A., Ballardini, R., Gandolfi, M.T., Balzani, V., Liu, Y., Northrop, B.H. and Stoddart, J.F. (2007) *J. Am. Chem. Soc.*, **129**, 4633.

40 Balzani, V., Credi, A. and Venturi, M. (1997) *Curr. Opin. Chem. Biol.*, **1**, 506.

41 Alpha, B., Balzani, V., Lehn, J.-M., Perathoner, S. and Sabbatini, N. (1987) *Angew. Chem. Int. Ed. Engl.*, **26**, 1266.

42 Bünzli, J.-C.G. and Piguet, C. (2005) *Chem. Soc. Rev.*, **34**.1048.

43 Blankenship, R.E. (2002) *Molecular Mechanism of Photosynthesis*, Blackwell Science, Oxford.

44 Balzani, V., Ceroni, P., Gestermann, S., Kauffmann, C., Gorka, M. and Vögtle, F. (2000) *Chem. Commun.*, 853.

45 Oar, M.A., Dichtel, W.R., Serin, J.M., Fréchet, J.M.J., Rogers, J.E., Slagle, J.E., Fleitz, P.A., Tan, L.-S., Ohulchanskyy, T.Y. and Prasad, P.N. (2006) *J. Am. Chem. Soc.*, **18**, 3682.

46 Yan, X., Goodson, T., III Imaoka, T. and Yamamoto, K. (2005) *J. Phys. Chem. B*, **109**, 9321.

47 Hecht, S. and Fréchet, J.M.J. (2001) *Angew. Chem. Int. Ed.*, **40**, 75.

48 Pleovets, M., Vögtle, F., De Cola, L. and Balzani, V. (1999) *New J. Chem.*, **23**, 63.

49 Balzani, V., Bergamini, G., Marchioni, F. and Ceroni, P. (2006) *Coord. Chem. Rev.*, **250**, 1254.

50 The dendrimer branches protect the excited state of the core also from quenching by other species: Vögtle, F., Plevoets, M., Nieger, M., Azzellini, G.C., Credi, A., De Cola, L., De Marchis, V., Venturi, M. and Balzani, V. (1999) *J. Am. Chem. Soc.*, **121**, 6290.

51 Goodsell, D.S. (2004) *Bionanotechnology – Lessons from Nature*, Wiley, Hoboken, NJ.

52 Jones, R.A.L. (2004) *Soft Machines, Nanotechnology and Life*, Oxford University Press, Oxford.

53 (a) Feynman, R.P. (1960) *Eng. Sci.*, **23**, 22. (b) Feynman, R.P. (1960) *Saturday Rev.*, **43**, 45. See alsohttp://www.feynmanonline.com.

54 See, e.g.: (a) Balzani, V., Credi, A., Langford, S.J., Raymo, F.M., Stoddart, J.F. and Venturi, M. (2000) *J. Am. Chem. Soc.*, **122**, 3542. (b) Jimenez-Molero, M.C., Dietrich-Bucheker, C. and Sauvage, J.-P. (2002) *Chem. Eur. J.*, **8**, 1456. (c) Badji,ć J.D., Balzani, V., Credi, A., Silvi, S. and Stoddart, J.F. (2004) *Science*, **303**, 1845. (d) Leigh, D.A., Lusby, P.J., Slawin, A.M.Z. and Walker, D.B. (2005) *Chem. Commun.*, 4919

55 Ballardini, R., Balzani, V., Credi, A., Gandolfi, M.T. and Venturi, M. (2001) *Acc. Chem. Res.*, **34**, 445.

56 See, e.g.: (a) Shinkai, S., Nakaji, T., Ogawa, T., Shigematsu, K. and Manabe, O. (1981) *J. Am. Chem. Soc.*, **103**, 111. (b) Irie, M. and Kato, M. (1985) *J. Am. Chem. Soc.*, **107**, 1024. (c) van Delden, R.A., Koumura, N., Schoevaars, A., Meetsma, A. and Feringa, B.L. (2003) *Org. Biomol. Chem.*, **1**, 33. (d) Leigh, D.A., Wong, J.K.Y., Dehez, F. and Zerbetto, F. (2003) *Nature*, **424**, 174. (e) Qu, D.-H., Wang, Q.-C. and Tian, H. (2005) *Angew. Chem. Int. Ed.*, **44**, 5296. (f) Muraoka, T., Kinbara, K. and Aida, T. 2006 *Nature*, **440**, 512

57 Credi, A. (2006) *Aust. J. Chem.*, **59**, 157.

58 Ballardini, R., Balzani, V., Credi, A., Gandolfi, M.T. and Venturi, M. (2001) *Int. J. Photoenergy*, **3**, 63.

59 Balzani, V., Credi, A., Marchioni, F. and Stoddart, J.F. (2001) *Chem. Commun.*, 1861.

60 Bissell, A., Córdova, E., Kaifer, A.E. and Stoddart, J.F. (1994) *Nature*, **369**, 133.

61 Schliwa M. (ed.) (2003) *Molecular Motors*, Wiley-VCH, Weinheim.

62 (a) Ballardini, R., Balzani, V., Gandolfi, M.T., Prodi, L., Venturi, M., Philp, D., Ricketts, H.G. and Stoddart, J.F. (1993) *Angew. Chem. Int. Ed.*, **32**, 1301. (b) Ashton, P.R., Ballardini, R., Balzani, V., Constable, E.C., Credi, A., Kocian, O., Langford, S.J., Preece, J.A., Prodi, L., Schofield, E.R., Spencer, N., Stoddart, J.F. and Wenger, S. (1998) *Chem. Eur. J.*, **4**, 2413. (c) Ashton, P.R., Balzani, V., Kocian, O., Prodi, L., Spencer, N. and Stoddart, J.F. 1998 *J. Am. Chem. Soc.*, **120**, 11190

63 Ashton, P.R., Ballardini, R., Balzani, V., Credi, A., Dress, R., Ishow, E., Kleverlaan, C.J., Kocian, O., Preece, J.A., Spencer, N., Stoddart, J.F., Venturi, M. and Wenger, S. 2000 *Chem. Eur. J.*, **6**, 3558.

64 Balzani, V., Clemente-León, M., Credi, A., Ferrer, B., Venturi, M., Flood, A.H. and Stoddart, J.F. (2006) *Proc. Natl. Acad. Sci. USA*, **103**, 1178.

65 For a related example of a photochemically driven molecular shuttle, see: Brouwer, A.M., Frochot, C., Gatti, F.G., Leigh, D.A., Mottier, L., Paolucci, F., Roffia, S. and Wurpel, G.W.H. (2001) *Science*, **291**, 2124.

66 Balzani, V., Clemente-León, M., Credi, A., Semeraro, M., Venturi, M., Tseng, H.-R., Wenger, S., Saha, S. and Stoddart, J.F. (2006) *Aust. J. Chem.*, **59**, 193.

67 Balzani, V., Credi, A., Silvi, S. and Venturi, M. (2006) *Chem. Soc. Rev.*, **35**, 1135.
68 Kay, E.R. and Leigh, D.A. (2006) *Nature*, **440**, 286.
69 Chatterjee, M.N., Kay, E.R. and Leigh, D.A. (2006) *J. Am. Chem. Soc.*, **128**, 4058.
70 For a representative recent example, see: Margulies, D., Felder, C.E., Melman, G. and Shanzer, A. (2007) *J. Am. Chem. Soc.*, **129**, 347.
71 (a) Rouvray, D. (2000) *Chem. Br.*, **36** (12), 46. (b) Ball, P. (2000) *Nature*, **406**, 118.
72 Requicha, A.A.G. (2003) *Proc. IEEE*, **91**, 1922.
73 Berná J., Leigh, D.A., Lubomska, M., Mendoza, S.M., Pérez, E.M., Rudolf, P., Teobaldi, G. and Zerbetto, F. (2005) *Nature Mater.*, **4**, 704.
74 Kocer, A., Walko, M., Meijberg, W. and Feringa, B.L. (2005) *Science*, **309**, 755.
75 de Silva, A.P., James, M.R., Mckinney, B.O.F., Pears, D.A. and Weir, S.M. (2006) *Nature Mater.*, **5**, 787.
76 Bhosale, S., Sisson, A.L., Talukdar, P., Furstenberg, A., Banerji, N., Vauthey, E., Bollot, G., Mareda, J., Roger, C., Würthner, F., Sakai, N. and Matile, S. (2006) *Science*, **313**, 84.

2
Rotaxanes as Ligands for Molecular Machines and Metal–Organic Frameworks

Stephen J. Loeb

2.1
Interpenetrated and Interlocked Molecules

2.1.1
Introduction

Interlocked molecules such as rotaxanes and catenanes (Figure 2.1) contain a fundamentally unique feature in chemical bonding: the *mechanical link*. As such, these threaded molecular species are not constrained by the normal conformational limits of standard organic molecules. The separate components of these mechanically linked organic nanostructures have an inherent freedom of motion that allows them to participate in large amplitude changes in overall structure. This concept has lead to the design of a vast array of molecular machines and nanoscale devices [1].

A variety of strategies exist for the synthesis of mechanically linked molecules. Probably the most common is the utilization of supramolecular assistance, which involves noncovalent interactions between a linear "axle" and a cyclic "wheel" to form an interpenetrated adduct known as a [2]pseudorotaxane (Figure 2.2) [2]. This initial assembly can be converted to a permanently interlocked [2]rotaxane by capping with bulky end groups or to a [2]catenane by linking the two ends of the linear axle. A wide variety of complementary components are capable of [2]pseudorotaxane formation in this manner, but there are only a handful of systems that are efficient at threading and can withstand significant structural modification. One of these, the [1,2-bis(pyridinium)ethane] $\subset$(24-crown-8) template is the subject of this chapter [3].

2.1.2
Templating of [2]Pseudorotaxanes

Examination of CPK and computer models suggested that the interaction of a 1,2-bis (pyridinium)ethane dication as the axle and a 24-membered crown ether as the wheel would give rise to an interpenetrated [2]pseudorotaxane structure. Indeed, detailed

Organic Nanostructures. Edited by Jerry L. Atwood and Jonathan W. Steed

ISBN: 978-3-527-31836-0

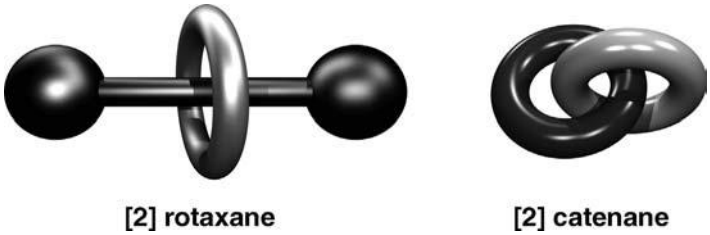

Figure 2.1 Cartoon depictions of simple examples of interlocked molecules: a [2]rotaxane (left) and a [2]catenane (right).

experiments showed that the combination of this new type of linear axle and a crown ether wheel such as 24-crown-8 (24C8), dibenzo-24-crown-8 (DB24C8) or dinaphtho-24-crown-8 (DN24C8) was an efficient and versatile templating method for the formation of [2]pseudorotaxanes. Nuclear magnetic resonance (^{1}H NMR) solution studies and solid-state X-ray structures showed clearly how the interpenetrated adducts are held together by $N^+ \cdots O$ ion–dipole interactions, a series of eight $CH \cdots O$ hydrogen bonds and, when available, significant π-stacking interactions between electron-poor pyridinium rings and electron-rich catechol rings (Figure 2.3) [4].

The strength of the noncovalent interactions could be controlled by varying the substituents on the axle pyridinium rings. It was demonstrated that an

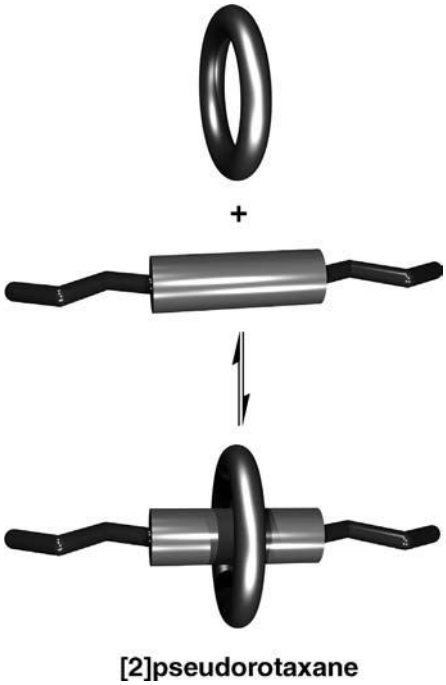

Figure 2.2 Cartoon outlining the equilibrium between an axle and wheel pair and an interpenetrated [2]pseudorotaxane.

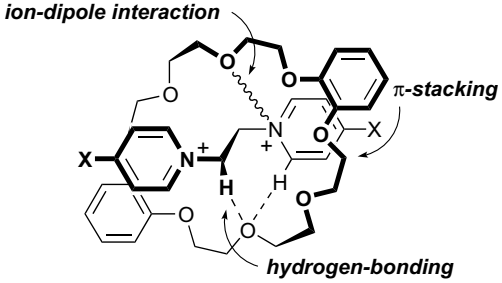

1a: X = H
1b: X = NH_2
1c: X = OMe
1d: X = Me
1e: X = Ph
1f: X = COOEt
1g: X = 4-Py
1h: X = BnPy

Figure 2.3 A schematic example of a [2]pseudorotaxane showing the noncovalent interactions that hold the axle and crown ether wheel together in an interpenetrated arrangement. The strength of these interactions can be fine tuned by the addition of EWG or EDG (X) and the presence of aromatic groups (benzo, naphtho) on the crown ether.

electron-withdrawing group provides increased hydrogen bonding and electrostatic interactions and therefore an increase in the stability of the adduct. Unlike the alkylammonium axles studied by Stoddart's group, which show their highest as sociation constants with 24C8, the 1,2-bis(pyridinium)ethane axles exhibit significant contributions from π-stacking and thus higher association constants with DB24C8. Association constants for a series of [2]pseudorotaxanes ranged from 10 to 4700 M^{-1} in MeCN-d_3 at 298 K [4]. Figure 2.4 shows the variation in association

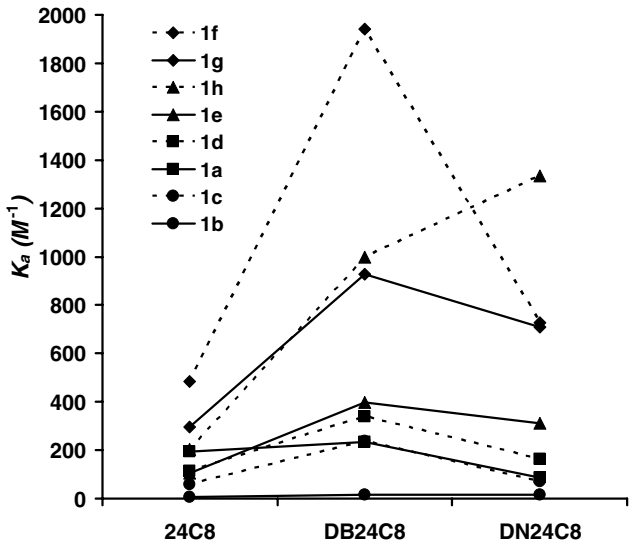

Figure 2.4 A plot showing the association constant for [2] pseudorotaxane formation (2×10^{-3} M, MeCN solution, 298 K) with variation in substituent at the 4-position on the pyridinium ring and crown ether.

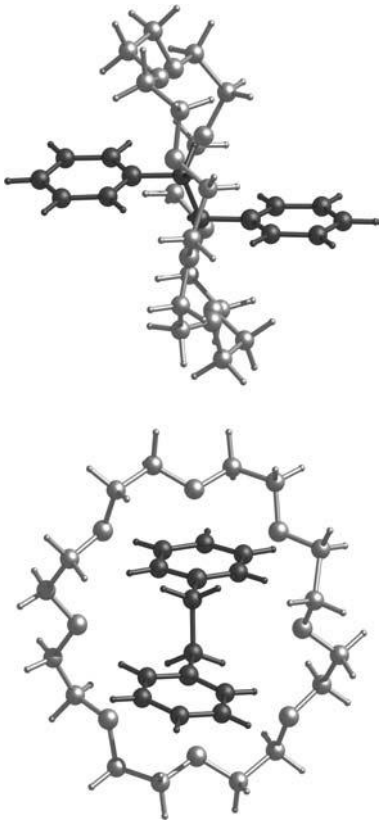

Figure 2.5 Two views of the interpenetration of axle and wheel in the X-ray structure of the simplest [2]pseudorotaxane, $[(\mathbf{1a}) \subset (24C8)]^{2+}$.

constant as a function of crown ether and substituent at the 4-position of the pyridinium ring. Figure 2.5 shows two views of the X-ray structure of the simplest [2]pseudorotaxane $[(\mathbf{1a}) \subset (24C8)]^{2+}$ containing the parent axle $\mathbf{1a}^{2+}$(R = H) and 24C8.

2.1.3 [2]Rotaxanes

The formation of [2]rotaxanes from [2]pseudorotaxanes involves the incorporation of bulky capping groups to prevent unthreading of the axle component from the wheel unit (Figure 2.6). This "threading-followed-by-capping" method has given rise to a number of synthetic capping strategies such as alkylation of amines and phosphines, ester, carbonate and acetal formation, oxidative coupling, cycloaddition and Wittig reactions [5].

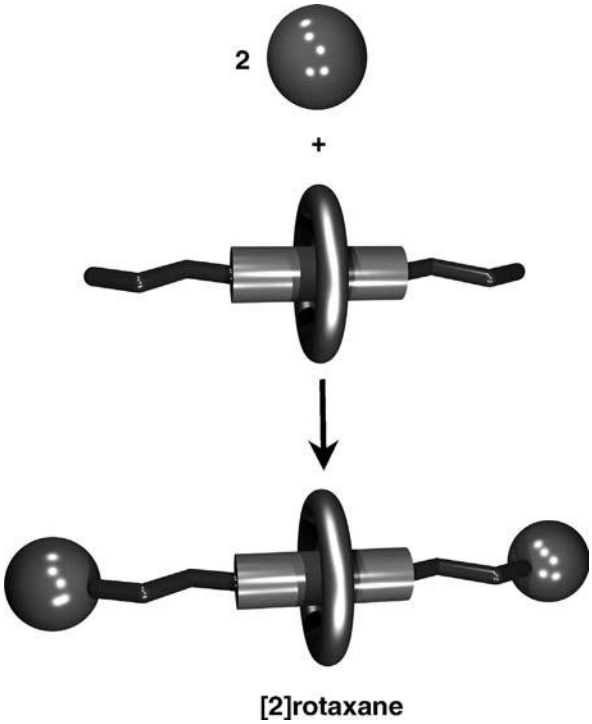

Figure 2.6 Cartoon outlining the conversion of an interpenetrated [2]pseudorotaxane into a permanently interlocked [2]rotaxane by capping with bulky groups.

We prepared the axle 1,2-bis(4,4′-bipyridinium)ethane, $\mathbf{1g}^{2+}$, which contains terminal pyridine groups. This allowed for the straightforward incorporation of a capping group by direct alkylation of the terminal pyridines to give axle $\mathbf{2}^{4+}$ and form the permanently interlocked [2]rotaxane $[(\mathbf{2}) \subset (\text{DB24C8})]^{4+}$. The *tert*-butylbenzyl group was employed as the cap as it was shown previously [4] that a pyridinium ring with a *t*-Bu substituent could not pass through DB24C8 [6]. The X-ray structures of the precursor [2]pseudorotaxane, $[(\mathbf{1g}) \subset (\text{DB24C8})]^{2+}$, and the resulting [2]rotaxane, $[(\mathbf{2}) \subset (\text{DB24C8})]^{4+}$, are shown in Figure 2.7.

The same methodology of threading-followed-by-capping can also be utilized to stopper the single terminal end of an axle that already contains a built-in bulky group. For example, [2]rotaxanes could also be prepared with a large triethylphosphonium group at one end; axle $\mathbf{3}^{3+}$. Figure 2.8 shows the X-ray structure of such a species [7].

2.1.4
Higher Order [*n*]Rotaxanes

Polyrotaxanes and polycatenanes are supramolecular polymers which contain macromolecular architectures built with mechanical linkages. Interest in these systems can be attributed to the fundamental role that interlocked components might play in

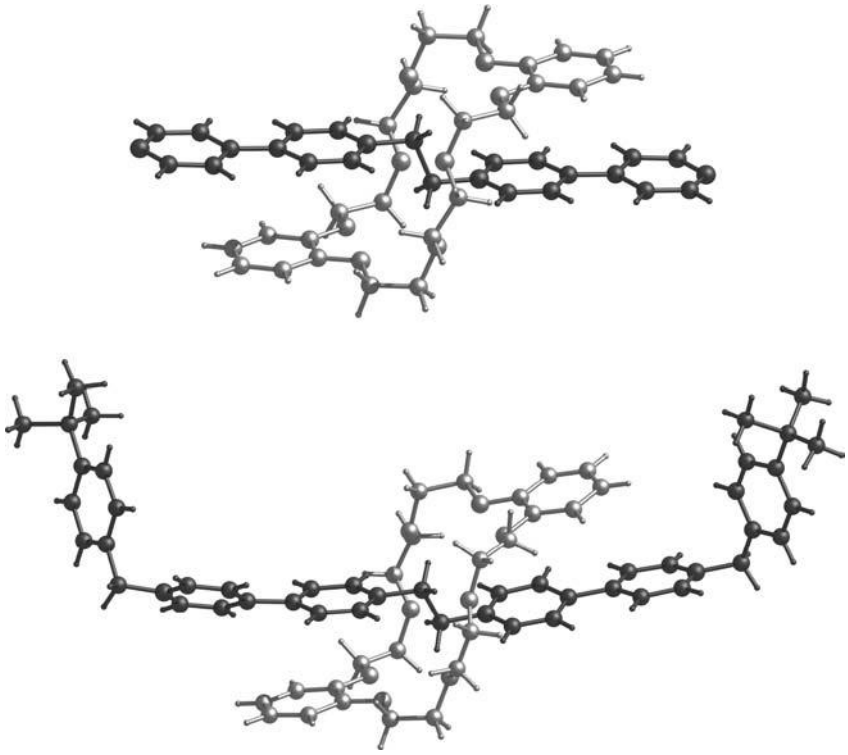

Figure 2.7 X-ray structures of the related [2]pseudorotaxane $[(\mathbf{1g}) \subset (24C8)]^{2+}$ and [2]rotaxane $[(\mathbf{2}) \subset (DB24C8)]^{4+}$.

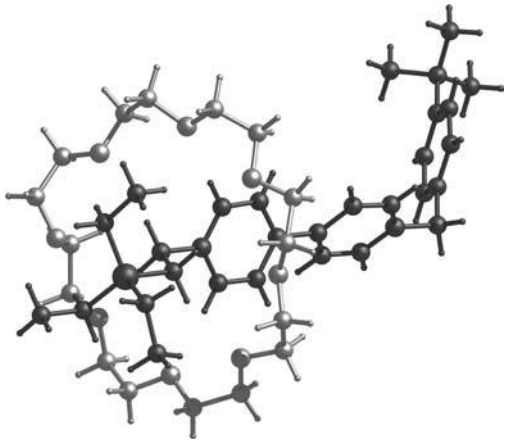

Figure 2.8 X-ray structure of the [2]rotaxane $[(\mathbf{3}) \subset (24C8)]^{3+}$ containing a large $-(PEt_3)^+$ phosphonium group.

the mechanical properties of polymers. Dendrimers and hyperbranched macromolecules based on interlocked components have also attracted recent attention as models for supramolecular polymers [8].

We were particularly interested in dendrimers in which all the branching points of the macromolecule are mechanical linkages. These can be constructed by either threading multiple ring components on to branches attached to a single core (Type A) or threading multiple axles on to rings appended to a central core (Type B) [9].

Initially we prepared extended axles containing two 1,2-bis(pyridinium)ethane-type binding sites. Threading multiple units of DB24C8 on to the axle followed by capping with *tert*-butylbenzyl groups gave Type A [3]rotaxanes [10].

Type B dendrimeric polyrotaxanes were prepared using multi-site crown ethers and multiple versions of axle $\mathbf{2}^{4+}$. Figure 2.9 shows an example of a [4]rotaxane prepared in this manner [10]. The product distribution of branched [*n*]rotaxanes

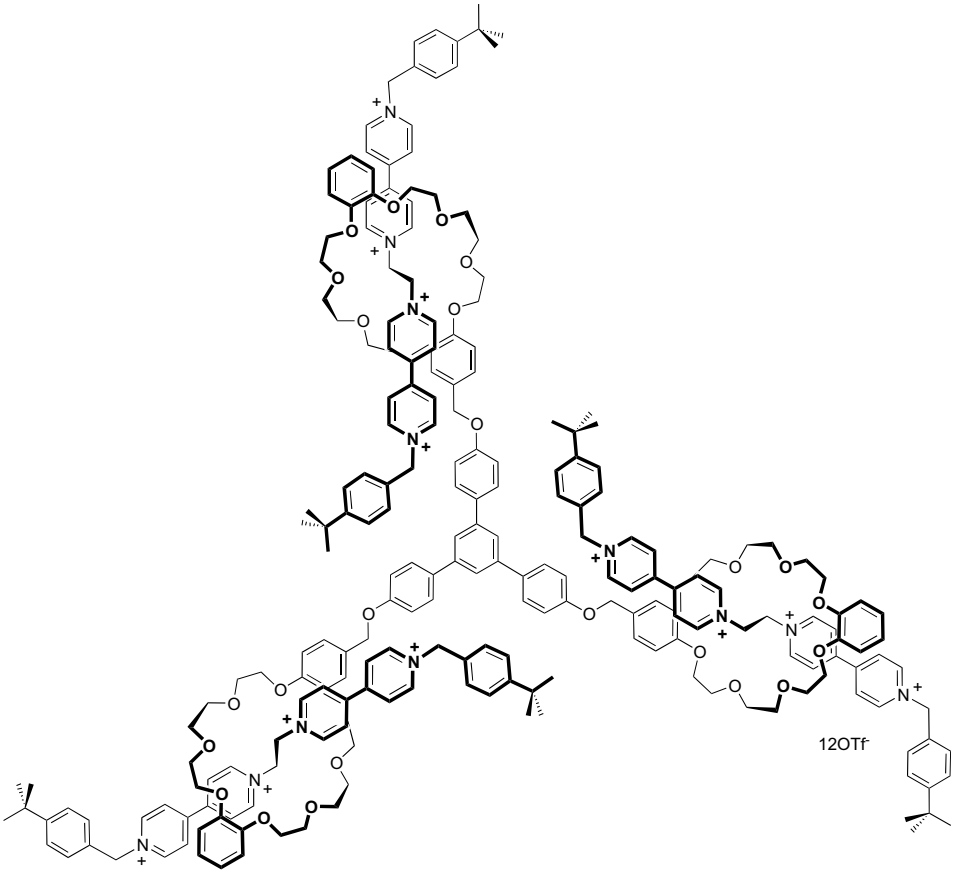

Figure 2.9 The tris(crown) ether with a 1,3,5-tris(4-hydroxyphenyl)benzene spacer allows the formation of a [4]rotaxane using axle $\mathbf{2}^{4+}$ containing *tert*-butylbenzyl capping groups.

observed gave a measure of the efficiency of the threading process. The size of the core could be a single benzene ring but this was only practical for the formation of two branches as the two crowns needed to be positioned away from each other in the 1,4-orientation to minimize inhibitory interactions [11]. The efficiency of the threading steps decreased sequentially and was attributed to three factors: (1) steric interactions between an already complexed crown ether site (pseudorotaxane or rotaxane) and the new incoming axle, (2) electrostatic repulsions between an existing rotaxane axle and the new incoming axle and (3) partial occupation of the unoccupied crown ether recognition elements by a neighboring rotaxane unit [11].

2.1.5
[3]Catenanes

The synthesis of complex interlocked assemblies such as $[n > 2]$catenanes, $[n > 2]$ molecular necklaces and $[n > 2]$rotacatenanes remains a considerable challenge for supramolecular chemists [1]. One of the major problems is that, regardless of design, there is always the requirement of forming at least one large ring during the self-assembly process. A potential strategy to aid ring closure involves the use of an external template, for example, a guest for a host catenane. During our studies on the (1,2-bis(pyridinium)ethane) $\subset$ (24-crown-8) templating motif, we discovered a unique one-step, self-assembly procedure for the preparation of [3]catenanes utilizing a terphenyl spacer unit that used DB24C8 as a very efficient template for the assembly of the [3]catenane containing this crown [12]. The X-ray structure in Figure 2.10

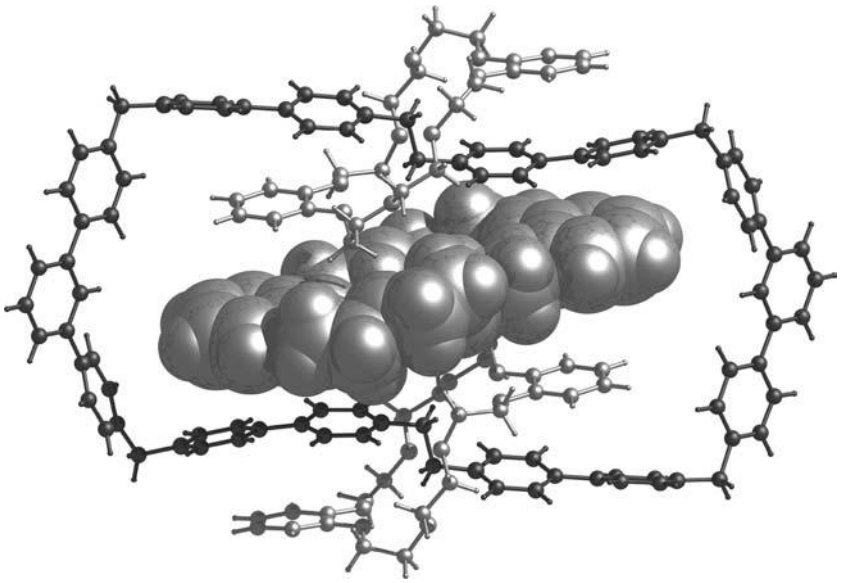

Figure 2.10 X-ray structure of the [3]catenane (ball-and-stick) that acts as host to an equivalent of DB24C8 (space-filling) as the guest.

shows how DB24C8 can act as a guest for the [3]catenane host, an interaction that can act to template the cyclization reaction and produce [3]catenane in good yield. The yield of the [3]catenane with DB24C8 (66%) was approximately twice that with any other crown ether studied, 24C8 (33%), B24C8 (35%), N24C8 (22%), BN24C8 (17%) and DN24C8 (23%), as only DB24C8 was a suitable guest [12].

2.2 Molecular Machines

2.2.1 Introduction

Control over the relative position and motion of components in interpenetrated or interlocked molecules can impart machine-like properties at the molecular level. Examples include threading and unthreading of a [2]pseudorotaxane, translation of the macrocycle in a [2]rotaxane molecular shuttle, rotation of the rings in a [2]catenane and reorientation (flipping, pirouetting) of the cyclic wheel in [2]rotaxanes [13].

2.2.2 Controlling Threading and Unthreading

During our study of [2]pseudorotaxane formation between 1,2-bis(pyridinium) ethane-type axles and 24-membered crown ether wheels, we noted that the presence of a strong EDG, such as NH_2, dramatically reduced the association constant [4]. This was attributed to a reduction in the acidity of the hydrogen bonding groups and a reduction in the charge at the pyridinium nitrogen due to contributions from an unfavorable resonance form. We then prepared an axle which could be represented by two resonance forms having dramatically different structures and charge distributions. This new axle had the structure of an organic D–π-A–π-D chromophore with two terminal donor groups (*N*,*N*-dimethylamino) and an inner acceptor group (bispyridinium), giving rise to an intramolecular charge transfer (ICT). It was possible to turn *OFF* the ICT by addition of a Lewis acid. X-ray crystal structures of the neutral and protonated forms as well as DFT (B3LYP) calculations verified the predicted resonance structures and electronic differences [14].

A substantial increase in association constant was observed for the protonated form compared to the unprotonated form. An ICT band with λ_{max} at 447 nm was observed in the absorption spectrum, but this intense orange color was completely eliminated upon addition of acid. The colorless, protonated axle then formed a [2]pseudorotaxane with DB24C8, which gave rise to a pale yellow coloration due to the weak charge-transfer interaction typical of $[(\mathbf{1}) \subset (\text{DB24C8})]^{2+}$ pseudorotaxanes (Figure 2.11).

The linking of this mechanical action of [2]pseudorotaxane formation to a significant color change can be described as a *NOT* logic gate since the threading

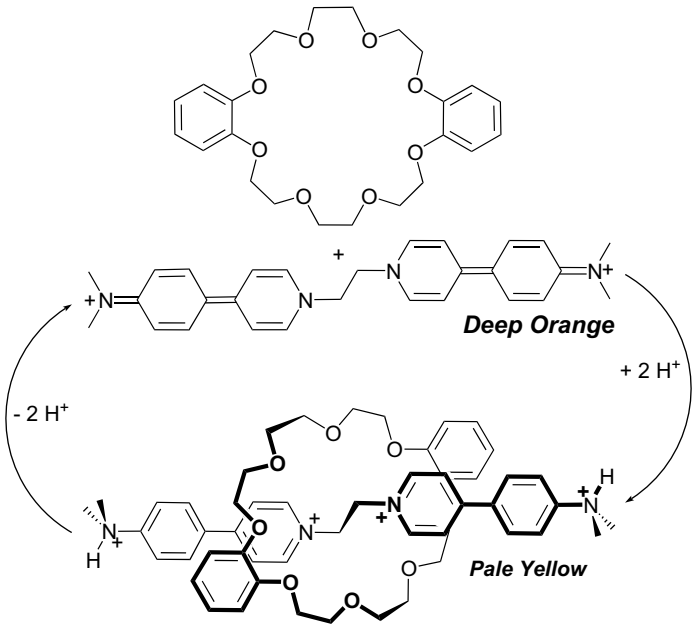

Figure 2.11 Schematic representation of the threading and unthreading process driven by alternating acid and base using an ICT axle.

of the two components to form the interpenetrated molecule is signaled by the loss of the orange color [14].

2.2.3 Molecular Shuttles

The transformation of mechanically linked molecules such as [2]rotaxanes and [2] catenanes into molecular machines requires the synthesis of systems with two or more distinct molecular arrangements (co-conformations) [13]. One of the most widely studied of these is the molecular shuttle pioneered by Stoddart's group [13]. In a molecular shuttle, two different recognition sites are present on the axle for the binding of a single macrocyclic wheel. The two states are translational isomers related by the relative positioning of the two interlocked components (Figure 2.12).

We utilized the axles from our [3]rotaxane study [15] to create molecular shuttles containing two binding sites of the 1,2-bis(pyridinium)ethane type for a single molecule of DB24C8 [16]. Since only one set of ^{1}H NMR resonances was observed for the axles at room temperature, it was concluded that the DB24C8 molecules were undergoing fast exchange between the two binding sites. From VT-NMR spectral data, it was determined that the rate of exchange between the two sites was on the order of 200–300 Hz. For the unsymmetrical species, the ratio of site occupancy was determined as 2 : 1.

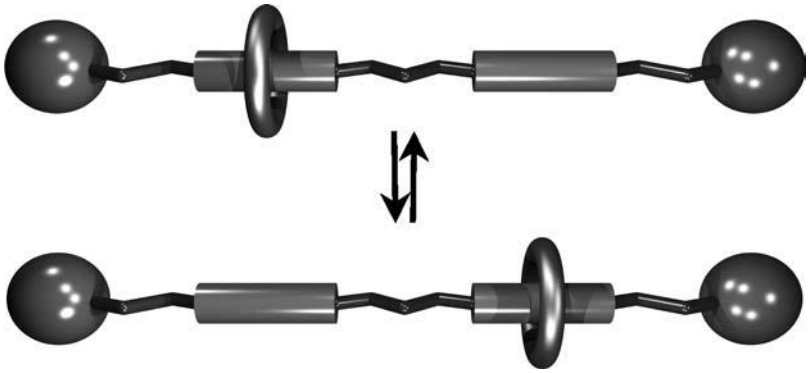

Figure 2.12 Cartoon depicting the two translational isomers of a [2]rotaxane molecular shuttle.

In order actually to control the motions of the components in these molecular shuttles, the 1,2-bis(pyridinium)ethane site was combined with an alkylammonium site which can be turned *ON* and *OFF* by protonation and deprotonation [17]. Figure 2.13 shows a molecular shuttle that operates as a bistable switch in dichloromethane solution by the sequential addition of acid and base. When the amine site is unprotonated there is no recognition element to interact with the crown ether and the [2]rotaxane is orange due to the same ICT absorption as found in our *ON*/*OFF* [2]

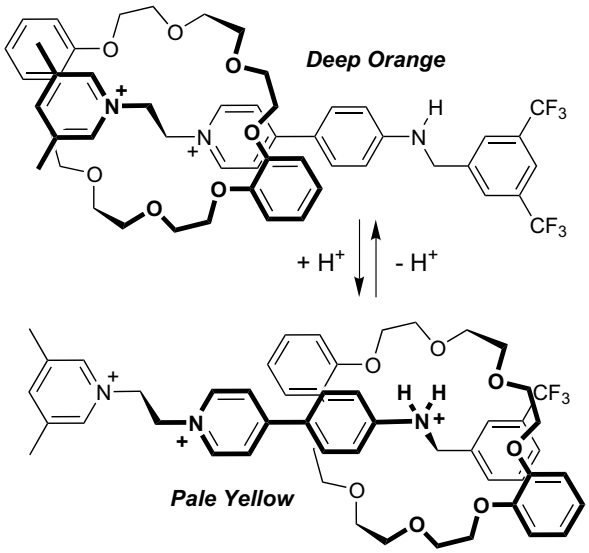

Figure 2.13 A molecular shuttle containing both 1,2-bis (pyridinium)ethane and benzylanilinium recognition sites that can be sensed optically and controlled by the addition of acid and base.

pseudorotaxane system described in Section 2.2.2. Upon protonation, a competition is established between the two sites which is dominated totally by the benzylanilinium recognition site [18] in a nonpolar solvent such as dichloromethane and there is complete elimination of the orange colored form due to quenching of the ICT absorption. This [2]rotaxane molecular shuttle is thus a bistable molecular switch that can be easily controlled by acid–base chemistry and observed by a simple optical read-out.

2.2.4
Flip Switches

We have demonstrated the existence of a new set of positional isomers based on [2]rotaxanes which contain a single recognition site but have different end groups on both the axle and crown ether wheel. The relative positioning of the two interlocked components produces two co-conformations and their reorientation is reminiscent of a mechanical "flip switch" (Figure 2.14) [19].

^{1}H NMR spectroscopy was used to determine that the populations of the two co-conformations were dependent upon the relative degrees of π-stacking between axle and wheel. Since solvent polarity is known to have a profound influence on intramolecular face-to-face π-stacking between aromatic rings [20], we studied a system with two different planar pyridinium groups of different surface area and demonstrated that the ratio of co-conformational isomers could be tuned by solvent polarity (Figure 2.15). The ratio of isomers showed an increase in π-stacking of the naphtho group with the 4,4′-bipyridinium group in more polar solvents. The X-ray structure of one of these [2]rotaxanes containing an unsymmetrical crown ether with both benzo and naphtho aromatic units, BN24C8, is shown in Figure 2.16.

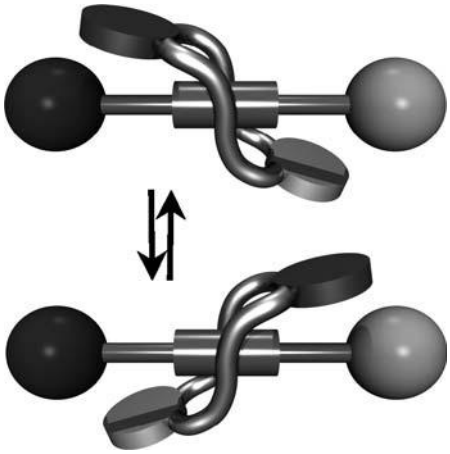

Figure 2.14 Cartoon illustrating the two co-conformations of a [2]rotaxane molecular flip-switch.

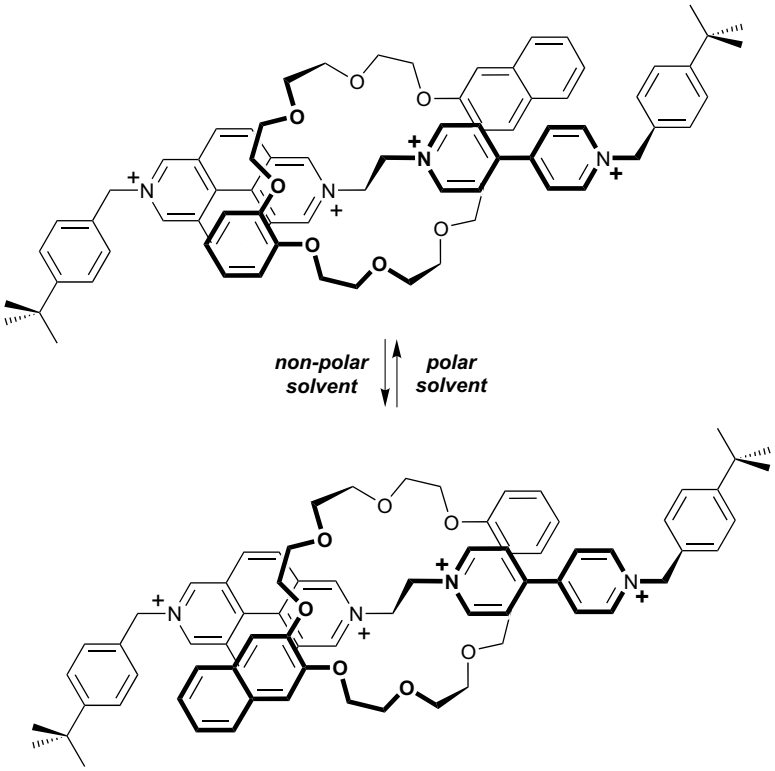

Figure 2.15 [2]Rotaxanes containing a 1,2-bis(pyridinium)ethane recognition site in which both the axle and wheel have different end groups can exist in two co-conformations that depend on the orientation of the components. The preference for a particular co-conformation is dependent upon π-stacking interactions and can be controlled by solvent polarity.

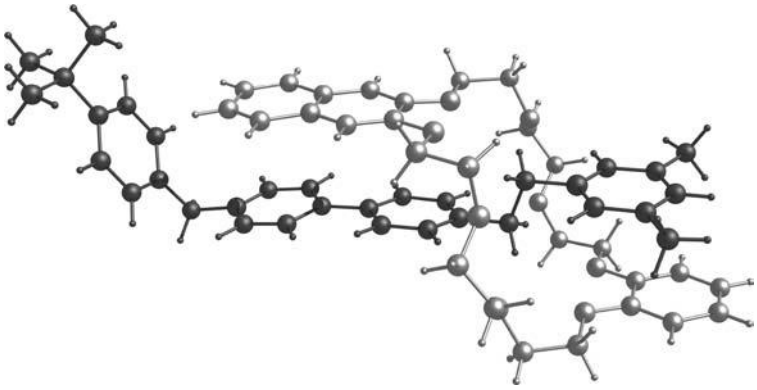

Figure 2.16 X-ray structure of a flip-switch molecule in the solid state. The co-conformation is that identified as the major one in solution with the larger naphtho ring π-stacked over the 4,4′-bipyridninium unit.

This new type of molecular switch with a single recognition site is just in its infancy but shows good potential. In particular, it is a very compact system and might be a good candidate for inclusion in solid-state devices in which large-amplitude changes in structure are more difficult to envision. Preliminary work in our laboratory has shown that the switching can be observed optically and the barrier to "flipping" controlled by inclusion of appropriate substituents on the axle and wheel [17].

2.3
Interlocked Molecules and Ligands

2.3.1
[2]Pseudorotaxanes as Ligands

Almost any metal complex with a single open coordination site is bulky enough to be used as an effective cap and form a metal-based [2]rotaxane. Our initial study involved using the axle $\mathbf{1g}^{2+}$ and DB24C8 to pre-form the [2]pseudorotaxane ligand followed by capping with the palladated pincer fragment $\{Pd[C_6H_3(CH_2SPh)_2]\}^+$ [10]. The ^1H NMR spectrum of the reaction mixture showed quantitative formation of the metal-capped [2]rotaxane which could be isolated from solution by crystallization; an X-ray structure verified the interlocked nature of the product. Subsequently, it was shown that the metal-containing caps could be larger, more sophisticated units such as the porphyrin complex [Ru(CO)(TTP)] [21] or simple anionic metal fragments such as $[MBr_3]_2$ (M = Mn, Co) [6]. The X-ray structures of the PdS_2- and $CoBr_3$-capped complexes are show in Figure 2.17.

2.3.2
[2]Rotaxanes as Ligands

One of the shortcomings of a self-assembly strategy for metal ion incorporation is that conditions for formation of the metal–ligand bonds must be compatible with maintaining the weaker noncovalent interactions between axle and wheel. A simple modification that circumvented this problem was replacement of one of the monodentate pyridine donors of $\mathbf{1g}^{2+}$ with a multidentate terpyridine group to give a new axle $\mathbf{3}^{3+}$. This gave rise to a series of permanently interlocked [2]rotaxanes containing 24C8, DB24C8 and DN24C8. Figure 2.18 shows the X-ray structure of the new interlocked ligand $[(\mathbf{3}) \subset (DN24C8)]^{3+}$ ready for coordination via the tridentate terpy site [22].

We then studied the coordination chemistry of $[(\mathbf{3}) \subset (24C8)]^{3+}$, $[(\mathbf{3}) \subset (DB24C8)]^{3+}$ and $[(\mathbf{3}) \subset (DN24C8)]^{3+}$ with Fe(II) [22] and Ru(II) [23]. Since the ligands are already [2]rotaxanes. the conditions under which coordination to a metal center is conducted do not effect the integrity of the mechanical linkage. For example, the Ru(II) complexes were prepared at reflux in polar solvents with no decomposition

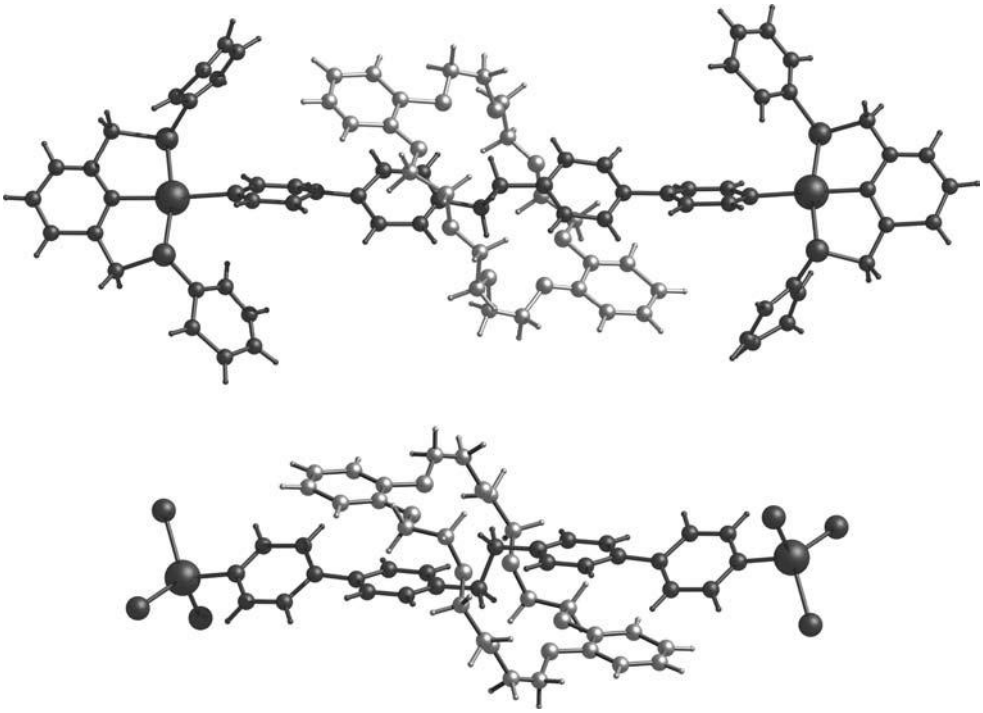

Figure 2.17 X-ray crystal structures of the two metal-based [2] rotaxanes derived from a combination of $\mathbf{1g}^{2+}$ and DB24C8 capped by (top) the palladated pincer fragments $[Pd(C_6H_3(CH_2SPh)_2)]^+$ and (bottom) the anionic fragments $CoBr_3$.

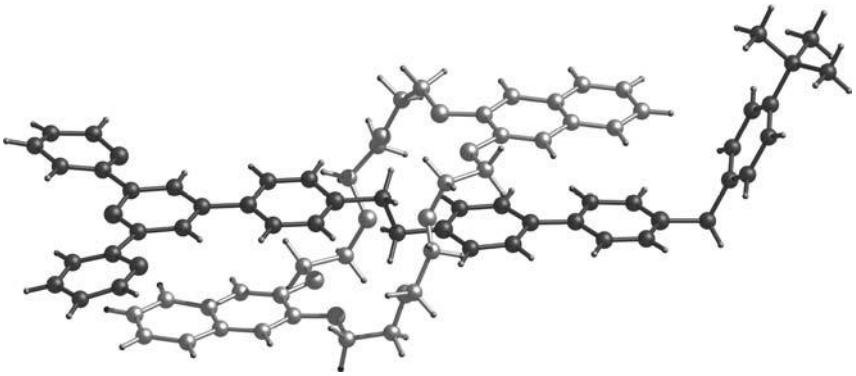

Figure 2.18 X-ray crystal structure of the [2]rotaxane ligand $\mathbf{3}^{3+}$ featuring a terpyridine chelating axle, capped with a *tert*-butylbenzyl group and containing DB24C8.

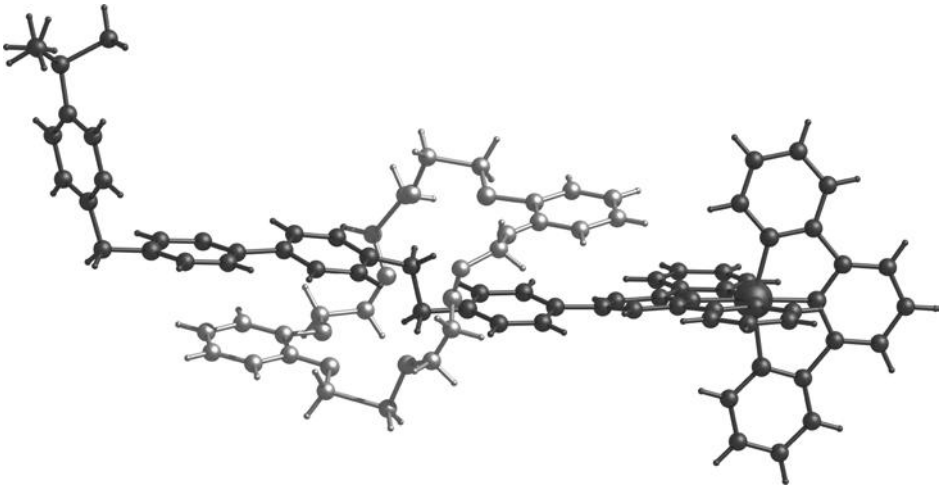

Figure 2.19 X-ray crystal structure of the Ru(II) complex of ligand $\mathbf{3}^{3+}$ formed with an equivalent of $[Ru(terpy)]^{2+}$.

of the [2]rotaxane ligands. Figure 2.19 shows an X-ray structure of the Ru(II) complex cation $\{(terpy)\ Ru[(\mathbf{3}) \subset (DB24C8)]\}^{5+}$ containing a chelating [2]rotaxane ligand.

A detailed investigation of the Ru(II) complexes showed some unique absorption and fluorescence properties that were dependent on the nature of the crown ether [23]. This synthetic approach has the potential to expand greatly the conditions under which metal complexes with mechanical linkages can be prepared and could produce a wide variety of [2]rotaxane metal complexes with unique electronic, magnetic or photo-physical properties [24].

2.4 Materials from Interlocked Molecules

2.4.1 Metal–Organic Rotaxane Frameworks (MORFs)

Although a great deal of information about the fundamental properties of mechanically interlocked molecules has been derived from solution studies [25,28], there still need to be methods for imposing order in these systems. Some ideas that have been studied are (i) attachment to surfaces (ii) tethering between electrodes (iii) incorporation into organic polymers [31] or dendrimers [9] and (iv) assembly into the repeating framework of a crystalline lattice The ultimate goal of this work is to produce materials that contain functional components that are addressable and controllable. We are interested in the solid state and in particular the formation of crystalline materials we have termed metal–organic rotaxane frameworks (MORFs) [33].

The use of simple [2]rotaxanes as linkers in MORF materials should provide a blueprint for the eventual inclusion of molecular machines into three-dimensional frameworks. For example, one defining attribute of a conventional metal–organic framework (MOF) material is the ability to modify the linker unit by organic synthesis [33]. With MORFs, an additional degree of flexibility is available as the rotaxane linker can be modified by retaining the axle unit but exchanging the wheel component. This *supramolecular* modification can potentially be used to tune the internal properties of the material [34].

The initial challenges that we have taken up and describe here are (1) the design of appropriate ligands, (2) the development of suitable synthetic routes and protocols for self-assembly and crystallization and (3) specific methods for materials characterization.

2.4.2 One-dimensional MORFs

The evolution from a [2]rotaxane capped with metal fragments to a 1D MORF was straightforward. Mixing $\mathbf{1g}^{2+}$ with an excess of DB24C8 in MeCN resulted in a solution which contained an equivalent of the [2]pseudorotaxane ligand. Diffusion of a solution of $[(\mathbf{1g}) \subset (DB24C8)]^{2+}$ (as the BF_4 salt) into an MeCN solution of $[M(H_2O)_6][BF_4]_2$ (M = Co, Zn) resulted in isolation of crystalline material with formula $\{Co(H_2O)_2(MeCN)_2(\mathbf{1g}) \subset (DB24C8))][BF_4]_4.(MeCN)_2(H_2O)_2\}_x$ (yields: 71% Co, 92% Zn).

The top structure in Figure 2.20 shows that the use of Co(II) ions in the presence of a coordinating solvent such as MeCN results in an octahedral coordination sphere comprised of two equivalents of $[(\mathbf{1g}) \subset (DB24C8)]^{2+}$, two MeCN molecules and two water molecules with each set of ligands having a *trans* orientation. The result is a coordination polymer in which every linker is a [2]rotaxane.

The linearity of the framework is due to the fact that $\mathbf{1g}^{2+}$ must adopt an *anti* conformation at the central ethylene unit when threaded through DB24C8. This structural feature combined with a *trans* geometry at the metal ion produces a linear 1D MORF with a Co···Co distance of 22.1 Å [35]. This polymer can be viewed as a metal–ligand "wire" in which the crown ethers act as a protective coating somewhat analogous to the use of long-chain hydrocarbons attached to phosphine ligands to surround metal–polyacetylene linkages [36]. This MORF also contains infinite channels parallel to the polymer chains which are filled with anions and solvent. The bottom structure in Figure 2.20 shows several strands of the framework. It is likely that the girth of this rotaxane ligand contributes both to the parallel organization of the chains and the channels between them. As evidence for this, we have crystallized two 1D polymers utilizing only $\mathbf{1g}^{2+}$ as the linker. In both cases, we observed a classic herringbone pattern; there was no parallel alignment of chains and neither compound contained void channels for solvent occlusion [35].

Figure 2.20 X-ray crystal structure a 1D MORF with Co(II) ion nodes and [(**1g**) ⊂ (DB24C8)]$^{2+}$ linkers showing (top) a single repeating unit and (bottom) two parallel strands.

2.4.3
Two-dimensional MORFs

Since the linear 1D MORFs contained an octahedral metal ion in which the ancillary ligands were solvent molecules, we reasoned that it should be possible to induce higher orders of dimensionality by employing a greater amount of $[(\mathbf{1g}) \subset (DB24C8)]^{2+}$ in a noncoordinating solvent. The reaction of two equivalents of $\mathbf{1g}^{2+}$ (as the BF_4 salt) with four equivalents of DB24C8 and one equivalent of $[M(H_2O)_6][BF_4]_2$ (M = Cu, Cd, Ni) in $MeNO_2$ produced X-ray quality crystalline material (average yields ~80%) [35]. The top structure in Figure 2.21 shows how the use of these metal ions in a non-coordinating solvent allows for a an octahedral coordination geometry comprising four $[(\mathbf{1g}) \subset (DB24C8)]^{2+}$ linkers in a square-planar arrangement, along with one water molecule and one coordinated BF_4 anion. The bottom structure shows how propagation of these units results in a 2D MORF with square nets and a formula $\{[Cd(H_2O)(BF_4)(\mathbf{1g}) \subset (DB24C8))_2][BF_4]_5(MeNO_2)_{15}\}_x$. The sides of the square are defined by Cd···Cd distances of 22.2 Å. The interlayer spacings are 12.0 and 10.0 Å with the layers stacked in a pattern that gives rise to an open framework material with large infinite channels lined with DB24C8 crown ethers. The channels are filled with anions and solvents; there are 15 molecules of $MeNO_2$ per Cd(II) ion. Calculations estimate that the accessible void space occupied by anions and solvent is 50%; 38% for solvent only [35].

2.4.4
Three-dimensional MORFs

Regardless of the metal to ligand ratio employed, a two-dimensional square net was the highest order MORF that could be attained using $[(\mathbf{1g}) \subset (DB24C8)]^{2+}$ as a bridging ligand. We ascribed the failure to obtain 3D frameworks to the hindrance involved in trying to place six sterically demanding ligands around a single transition metal ion. In order to avoid crowding at the metal center, we made two changes: (1) we synthesised the bis-*N*-oxide analogue of $\mathbf{1g}^{2+}$, a new axle $\mathbf{4}^{2+}$, which allowed the formation of a new linker $[(\mathbf{4}) \subset (DB24C8)]^{2+}$, and (2) we employed larger lanthanide metal ions.

Three equivalents of $\mathbf{4}^{2+}$ (as the OTf salt) were reacted with nine equivalents of DB24C8 and one equivalent of $[M(OTf)_3]$ (M = Sm, Eu, Gd, Tb) in MeCN. X-ray quality crystalline material was produced in moderate yield (average yields ~50%). The top structure in Figure 2.22 shows that the use of Ln(III) ions as nodes results in an eight-coordinate metal center with a square *anti*-prismatic geometry comprised of six $[(\mathbf{4}) \subset (DB24C8)]^{2+}$ linkers, one water molecule and one coordinated triflate anion [37]. The bottom structure shows how propagation of these units results in 3D MORFs with formula $\{[M(H_2O)(OTf)(\mathbf{4}) \subset (DB24C8))_3][Cl][OTf]_7.(2MeCN)\}_x$ (M = Sm, Eu, Gd, Tb) in which every linker is a [2]rotaxane. The edges of the "cube" are defined by Sm···Sm distances of ~23.5 Å. Although the internal cavity of this 3D framework has a volume of ~10 000 Å [3], this apparently void space is filled by the single interpenetration of a parallel net. This is an obvious side-effect of employing

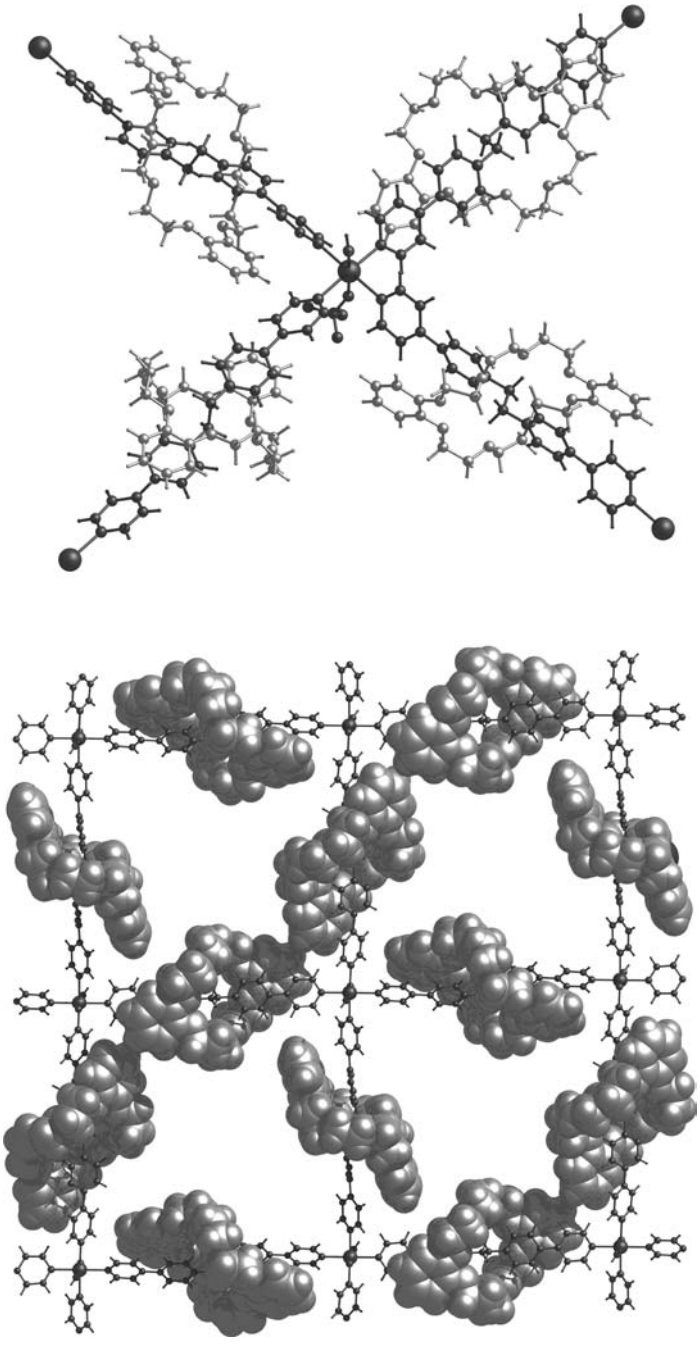

Figure 2.21 X-ray crystal structure a 2D MORF with Cd(II) ion nodes and [(**1g**) ⊂ (DB24C8)]$^{2+}$ linkers showing (top) the coordination sphere around a single metal ion and (bottom) a portion of the 2D square net.

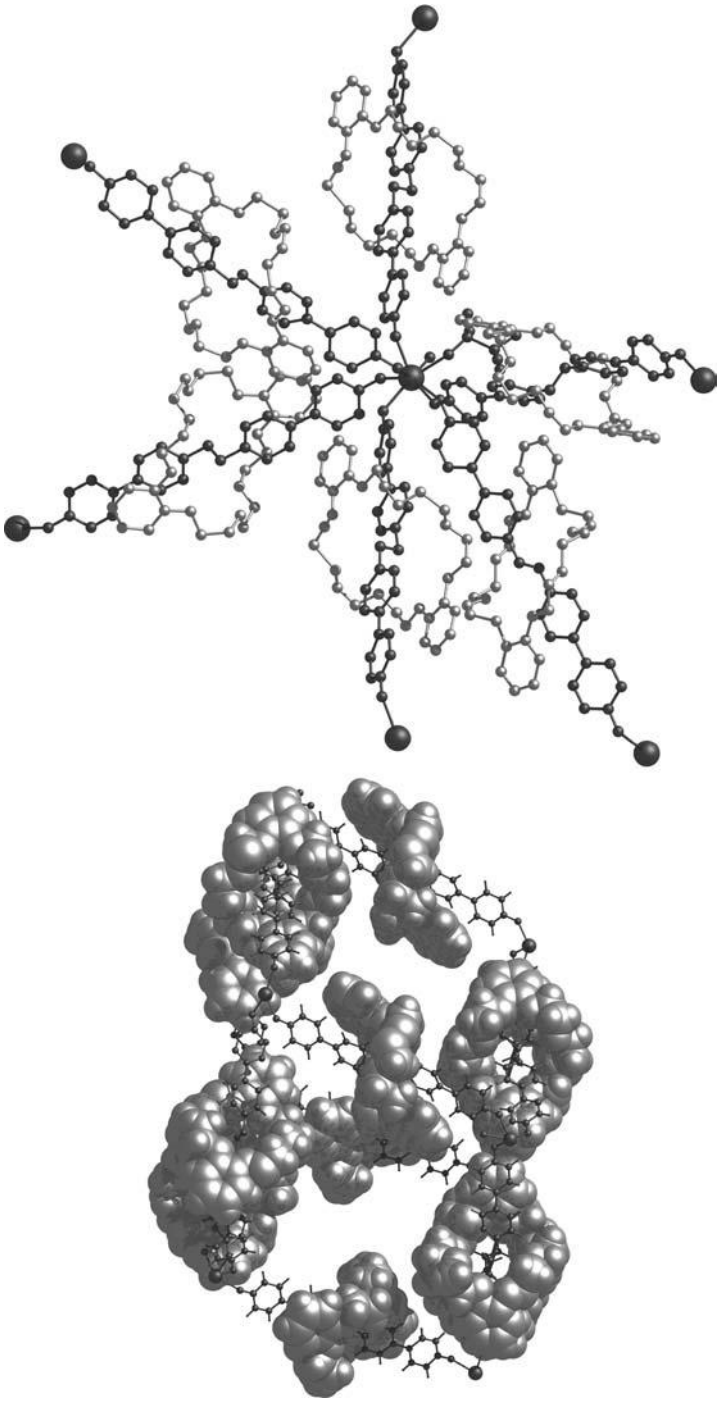

Figure 2.22 X-ray crystal structure a 3D MORF with Sm(III) ion nodes and $[(\mathbf{4}) \subset (DB24C8)]^{2+}$ linkers showing (top) the coordination sphere around a single metal ion and (bottom) a portion of the α-Po-type framework.

the longer axles and increasing the metal–metal distance. This creates an expanded cavity with larger "windows" which can now accommodate the girth of the [2]rotaxane ligand and allow interpenetration to occur.

An isomorphous series of 3D MORFs (Sm, Eu, Gd, Tb) based on eight-coordinate metal centers was possible, but changing to a smaller lanthanide ion, Yb(III) (2.40 vs. 2.51 Å, for Tb), yielded a completely different MORF. A material with formula $\{[Yb(OTf)(\mathbf{4}) \subset (DB24C8))_3][Cl][OTf]_7\}_x$ was isolated in moderate yield using the same diffusion procedure as used to produce the other 3D MORFs. In this case, a unique seven-coordinate pentagonal bipyramidal geometry was adopted by the smaller Yb (III) center. Five *N*-oxide-based rotaxanes occupy the five equatorial sites of the pentagonal plane with a sixth rotaxane and a single triflate ion positioned in the two axial sites, as shown in the top structure in Figure 2.23. Upon reducing the size of the Ln(III) node, a single water molecule is removed and the coordination number decreased from eight to seven. This subtle change has a dramatic effect on the nature of the resulting MORF structure [37]. Since the novel seven-coordinate geometry at Yb(III) contains a pentagonal equatorial plane and close-packed tiling in two dimensions with pentagons is impossible, it was interesting to see how this dilemma was circumvented. What occurs is that each *N*-oxide ligand "bends" at the Yb−O−N linkage, so a (3/4,5) net is formed, which solves the tiling problem by utilizing a combination of alternating triangles and squares rather than pentagons. Until very recently, this two-dimensional pattern was unknown in chemical systems [38]. The bottom structure in Figure 2.23 shows the tiling in the pentagonal plane. This network propagates one step further into a full 3D MORF by pillaring to alternating layers utilizing the sixth $[(\mathbf{4}) \subset (DB24C8)]^{2+}$ ligand in the apical position. This results in a previously unknown chemical topology which takes the form of a (3/4/6,6) six-connected net comprised of triangles, squares and hexagons. The square openings are used for interpenetration as this is not possible through the more crowded triangular cavities.

2.4.5
Controlling the Dimensionality of a MORF

Attempts to construct a 3D MORF with $[(\mathbf{4}) \subset (DB24C8)]^{2+}$ using smaller transition metal ions such as Cd(II) did yield a polyrotaxane but not the desired 3D framework. Instead, a 2D network was created with only one of the directions utilizing $[(\mathbf{4}) \subset (DB24C8)]^{2+}$ and the other simply employing a "naked" $\mathbf{4}^{2+}$ as a linker with no crown ether wheel [39]. The bottom structure in Figure 2.24 shows the basic coordination sphere around the Cd(II) center.

The X-ray crystal structure of the MORF material shows that the solid has the formula $\{[Cd(\mathbf{4}) \subset (DB24C8))(\mathbf{4})(OTf)_2][OTf]_4(MeNO_2)_4\}_n$. The Cd(II) metal centers adopt an octahedral geometry with three different pairs of ligands in an all-*trans* arrangement. Two rotaxane ligands and two "naked" axles define a square plane while two triflate anions are in the axial positions. This is similar to the Cd(II) MORF prepared using the pyridine-based rotaxane ligand $[(\mathbf{1g}) \subset (DB24C8)]^{2+}$. In that structure, the cavities of the grid were aligned to

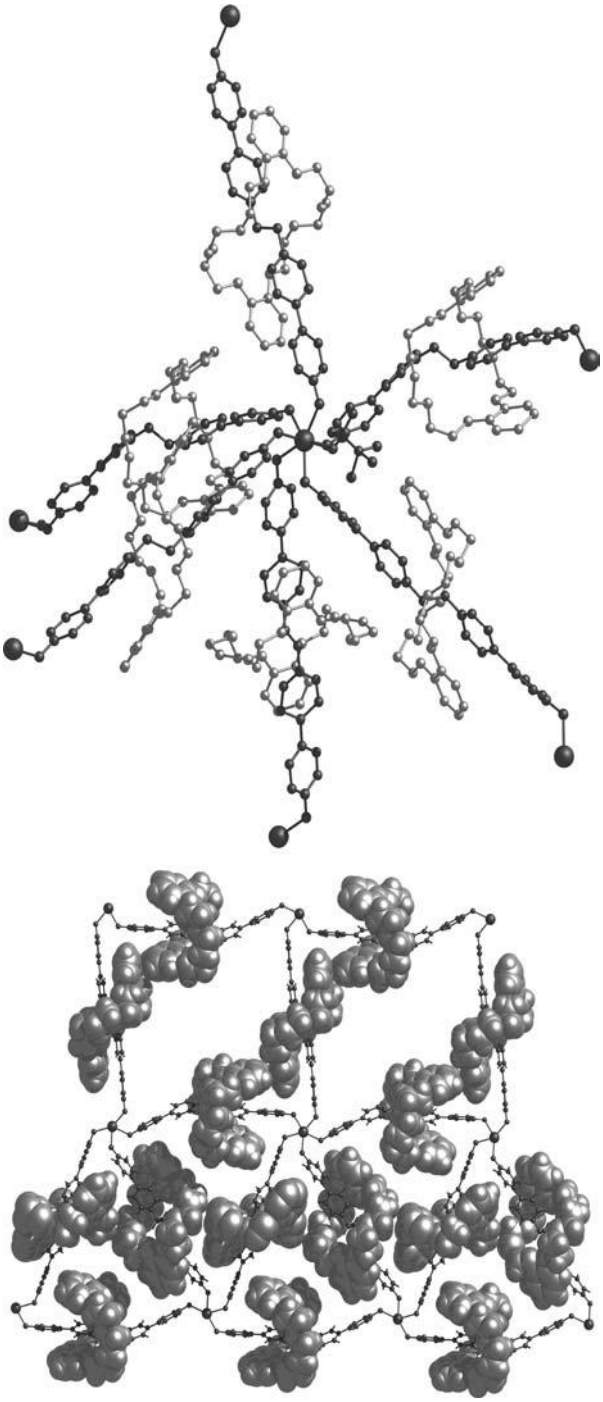

Figure 2.23 X-ray crystal structure a 3D MORF with Yb(III) ion nodes and [(**4**) ⊂ (DB24C8)]$^{2+}$ linkers showing (top) the unique 2D network comprised of square and triangular units.

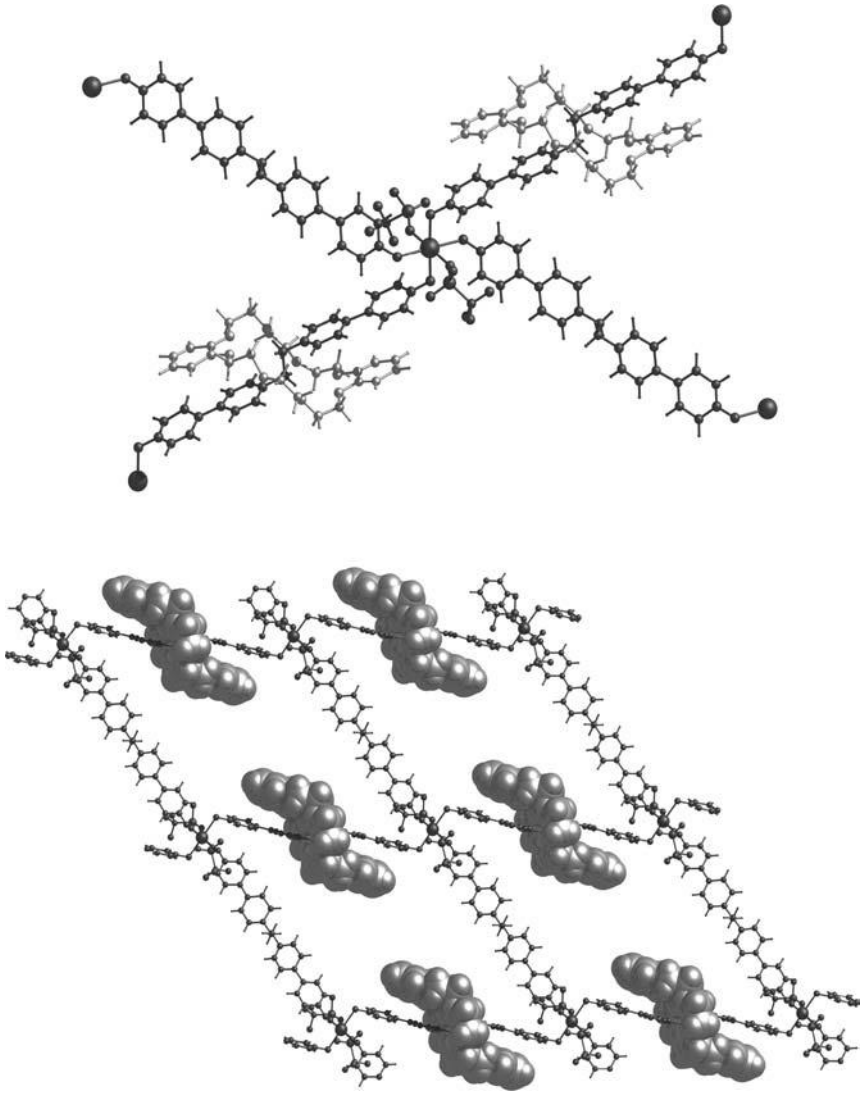

Figure 2.24 X-ray crystal structure of the pillared 1D MORF with Cd(II) ion nodes with $[(\mathbf{4}) \subset (DB24C8)]^{2+}$ rotaxane linkers and naked $\mathbf{4}^{2+}$ pillars showing (top) the coordination sphere around a single Cd(II) ion and (bottom) a portion of the polar 2D network.

produce large channels filled with solvent [35]. However, in this new structure, each cavity is filled by crown ethers from the layers above and below. The network is actually reminiscent of the 1D MORF structure based on Co(II) or Zn (II) and $[(\mathbf{1g}) \subset (DB24C8)]^{2+}$ as it can be thought of as a pillared 1D MORF. That is, the two *trans*-oriented $[(\mathbf{4}) \subset (DB24C8)]^{2+}$ linkers coordinate to the Cd(II)

center in one dimension while the two $\mathbf{4}^{2+}$ molecules pillar the polyrotaxane strands in the second dimension (see the bottom structure in Figure 2.24).

Finally, a property of this new MORF that is intriguing is its crystallization in the noncentrosymmetric space group *P*1. All the crown ether wheels are oriented in the same fashion along each strand of the grid. This is significant as it may be possible to replace DB24C8 with substituted crown ethers and thus orient all the wheel dipoles in the same direction by virtue of their entrapment on the metal–ligand grid. This may have potential as a novel method for creating NLO or similar materials that require ordering of functional groups by taking advantage of this supramolecular modification.

2.4.6
Frameworks Using Hydrogen Bonding

Since we had success in using metal ions as nodes to build MORFs, we looked at the possibility of using hydrogen bonding for the systematic preparation of solid-state materials which contain mechanical linkages. In this vein, we have shown that H^+ can be used in place of a metal ion to form polymeric systems with formula $\{[(H_2\mathbf{1g}) \subset (DB24C8)(DB24C8)][OTf]_4\}_x$ via hydrogen bonding [40]. In a single-stranded 1D MORF structure, the diprotonated [2]pseudorotaxane $[(H_2\mathbf{1g}) \subset (DB24C8)]^{4+}$ acts as the H-bond donor while a second equivalent of DB24C8 acts as the H-bond acceptor. The bottom structure in Figure 2.25 shows this H-bonded pair, and the bottom structure shows how this motif extends into a polymeric structure with parallel strands.

2.5
Properties of MORFs: Potential as Functional Materials

2.5.1
Robust Frameworks

All of the MORF materials prepared to date show the same basic stability. They are highly crystalline materials that occlude solvent to some degree and each loses some portion of the trapped solvent rapidly upon removal from the mother liquor at room temperature. Thermogravimetric analysis showed that all residual solvent was removed after heating to ~100°C. Each MORF studied then showed a stable phase until ~225–250°C, at which point decomposition of the metal–ligand framework was indicated by loss of DB24C8. It should be noted that the interlocked crown ether, although originally held in place by weak noncovalent bonds, can only be removed by breaking a covalent bond in the metal–ligand backbone. Thus, the loss of DB24C8 is actually a sensitive and unambiguous detection of framework breakdown.

In the case of the 3D MORFs, powder XRD patterns of the stable desolvated phase were consistent with retention of the 3D framework observed in the

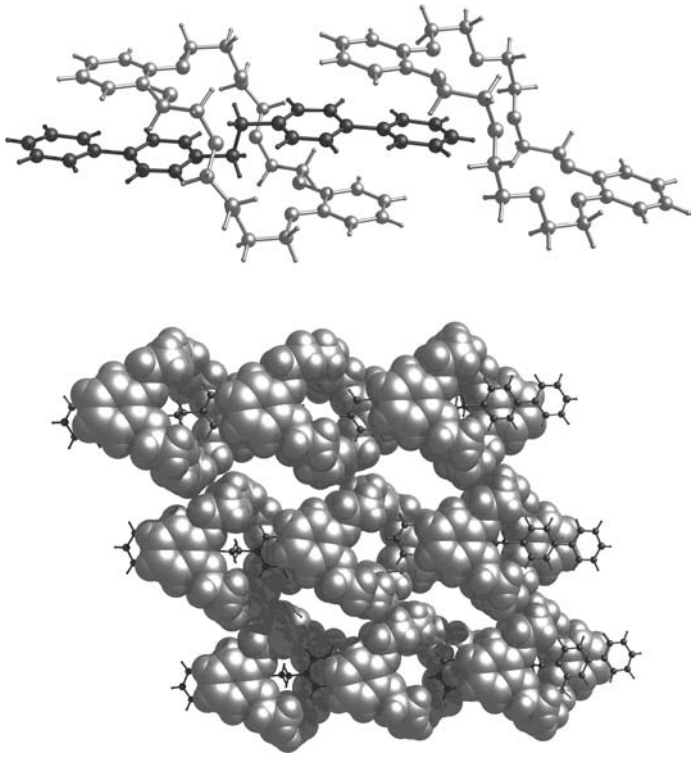

Figure 2.25 X-ray crystal structure of the 1D MORF with alternating $[(\mathbf{1g}) \subset (DB24C8)]^{2+}$ units and DB24C8 held together by hydrogen bonding showing (top) the repeating unit and (bottom) three parallel strands.

single-crystal structures. Although the 1D and 2D materials do not retain their original lattices, the polyrotaxane frameworks remain intact, as evidenced by the observation of a stable phase over a ~150°C range prior to loss of crown ether. We can confidently conclude that these new materials are at least as stable as basic coordination polymers and there is nothing inherently unstable about a MORF structure.

For this chemistry to evolve, we must be able to prepare truly robust MORFs. This is an issue that can be addressed by utilizing stronger metal–ligand interactions and metal clusters as nodes following the well-documented evolution of conventional MOF materials. We have already shown that rotaxane ligands such as $[(\mathbf{3}) \subset (DB24C8)]^{3+}$, with a terpy chelator, will allow metal complexation under extreme synthetic conditions. This type of approach should therefore greatly extend the synthetic conditions under which MORF assembly can be conducted and allow the preparation of materials with increased stability.

2.5.2
Porosity and Internal Properties

The challenge of creating porous MOF materials for a variety of applications such as gas storage and catalysis is ongoing and some tremendous progress has been made [41]. One of the contributions that MORF materials can make to this area is fine tuning the internal properties of porous materials. For a conventional MOF, the properties of the internal cavities or channels are dictated by the chemical structure of the organic linkers which define the great majority of the internal surface area. In a MORF, this internal surface is primarily related to the nature of the cyclic component and not the linking backbone. So, when a robust and porous MORF can be created, the axle and metal nodes will dictate the shape of the framework but the cyclic wheel will define the internal surface chemistry. It should then be a facile supramolecular event to replace, for example, hydrophobic groups on the exterior of one wheel with hydrophilic groups of another and thereby change the internal property of the material in a predictable fashion without altering the framework of the MORF.

2.5.3
Dynamics and Controllable Motion in the Solid State

One of the ultimate goals of MORF chemistry is to create solid-state materials that contain arrays of ordered molecular machines based on mechanically interlocked species. We have already created the molecules and observed their properties in solution and learned how to create basic MORF structures. The next step in the development of these materials will be to prepare robust, crystalline materials with mechanically switchable components [42]. The ultimate result could be bulk materials with individual components that can be individually addressed by simple external signals (chemical, electrochemical, photochemical, etc.), thus combining the chemistry of molecular machines and the properties of solid-state materials.

References

1 Arico, F., Badjic, J.D., Cantrill, S.J., Flood, A.H., Leung, K.C.-F., Liu, Y. and Stoddart, J.F. (2005) *Top. Curr. Chem.*, **249**, 203, and references therein.

2 Fyfe, M.C.T., Stoddart, J.F. and Fraser, J. (1997) *Acc. Chem. Res.*, **30**, 393.

3 Loeb, S.J. and Wisner, J.A. (1998) *Angew. Chem. Int. Ed.*, **37**, 2838.

4 (a) Loeb, S.J., Tiburcio, J., Vella, S.J. and Wisner, J.A. (2006) *Org. Biomol. Chem.*, **4**, 667. (b) Loeb, S.J. and Wisner, J.A. (1998) *Chem. Commun.*, 2757.

5 (a) Ashton, P.R., Chrystal, E.J.T., Glink, P.T., Menzer, S., Schiavo, C., Spencer, N., Stoddart, J.F., Tasker, P.A., White, A.J.P. and Williams, D.J. (1996) *Chem. Eur. J.*, **2**, 709. (b) Ashton, P.R., Bartsch, R.A., Cantrill, S.J., Hanes, R.E. Jr., Hickingbottom, S.K., Lowe, J.N., Preece, J.A., Stoddart, J.F., Talanov, V.S. and

Wang, Z.-H. (1999) *Tetrahedron Lett.*, **40**, 3661.
6 Davidson, G.J.E., Loeb, S.J., Parekh, N.A. and Wisner, J.A. (2001) *Dalton Trans.*, 3135, and references therein.
7 Georges, N., Loeb, S.J., Tiburcio, J. and Wisner, J.A. (2004) *Org. Biomol. Chem.*, **2**, 2751.
8 Huang, F. and Gibson, H.W. (2005) *Prog. Polym. Sci.*, **30**, 982 and references therein.
9 Lee, J.W. and Kim, K. (2003) *Top. Curr. Chem.*, **228**, 111, and references therein.
10 Loeb, S.J. and Wisner, J.A. (1998) *Chem. Commun.*, 2757.
11 Loeb, S.J. and Tramontozzi, D.A. (2005) *Org. Biomol. Chem.*, **3**, 1393.
12 Hubbard, A.L., Davidson, G.J.E., Patel, R.H., Wisner, J.A. and Loeb, S.J. (2004) *Chem. Commun.*, 138.
13 Balzani, V., Credi, A., Raymo, F.M. and Stoddart, J.F. (2000) *Angew. Chem. Int. Ed.*, **39**, 3348.
14 Vella, S.J., Tiburcio, J., Gauld, J.W. and Loeb, S.J. (2006) *Org. Lett.*, **8**, 3421.
15 Loeb, S.J. and Wisner, J.A. (2000) *Chem. Commun.*, 845.
16 Loeb, S.J. and Wisner, J.A. (2000) *Chem. Commun.*, 1939.
17 Vella, S.J. (2006) PhD Thesis, University of Windsor, Windsor, ON.
18 Vella, S.J., Tiburcio, J. and Loeb, S.J. (2005) *Org. Lett.*, **7**, 4923.
19 Loeb, S.J., Tiburcio, J. and Vella, S.J. (2006) *Chem. Commun.*, 1598.
20 Hunter, C.A. (2004) *Angew. Chem., Int. Ed.*, **43**, 5310.
21 Chichak, K., Walsh, M.C. and Branda, N.R. (2000) *Chem. Commun.*, 847.
22 Davidson, G.J.E. and Loeb, S.J. (2003) *Dalton Trans.*, 4319.
23 Davidson, G.J.E., Loeb, S.J., Passaniti, P., Silvi, S. and Credi, A. (2006) *Chem. Eur. J.*, **12**, 3233.
24 Bonnet, S., Collin, J.-P., Koizumi, M., Mobian, P. and Sauvage, J.-P. (2006) *Adv. Mater.*, **18**, 1239, and references therein.
25 Pease, A.R., Jeppesen, J.O., Stoddart, J.F., Luo, Y., Collier, C.P. and Heath, J.R. (2001) *Acc. Chem. Res.*, **34**, 433.
26 Collin, J-.P., Dietrich-Buchecker, C., Gaviña, P., Jiminez-Molero, M.C. and Sauvage, J.-P. (2001) *Acc. Chem. Res.*, **34**, 477.
27 Shipway, A.N. and Willner, I. (2001) *Acc. Chem. Res.*, **34**, 421.
28 Ballardini, R., Balzani, V., Credi, A., Gandolfi, M.T. and Venturi, M. (2001) *Acc. Chem. Res.*, **34**, 445, and references therein.
29 Tseng, H.-R., Wu, D., Fang, N.X., Zhang, X. and Stoddart, J.F., (2004) *ChemPhysChem* **5**, 111 and references therein.
30 Yu, H., Luo, Y., Beverly, K., Stoddart, J.F., Tseng, H.-R. and Heath, J.R. (2003) *Angew. Chem. Int. Ed.*, **42**, 5706.
31 Gibson, H.W., Nagvekar, D.S., Yamaguchi, M., Bhattacharjee, S., Wang, H., Vergne, M.J. and Hercules, D.M. (2004) *Macromolecules*, **37**, 7514, and references therein.
32 Yaghi, O.M., O'Keefe, M., Ockwing, N.W., Chae, H.K., Eddaoudi, M. and Kim, J. (2003) *Nature*, **423**, 705, and references therein.
33 Loeb, S.J. and Wisner, J.A. (2005) *Chem. Commun.*, 1511. The term MORF is used in this article to designate a sub-class of MOF as defined by Yaghi; See Rowsell, J.L. C. and Yaghi, O.M. (2004) *Microporous Mesoporous Mater.*, **73**, 3.
34 The preparation of these materials pre-dates those described herein. For an excellent review of this chemical system, see. Kim, K. (2002) *Chem. Rev.*, **31**, 96
35 Davidson, G.J.E. and Loeb, S.J. (2003) *Angew. Chem. Int. Ed.*, **42**, 74.
36 Stahl, J., Bohling, J.C., Bauer, E.B., Peters, T.B., Mohr, W., Martín-Alvarez, J.M., Hampel, F. and Gladysz, J.A. (2002) *Angew. Chem. Int. Ed.*, **41**, 1872, and references therein.
37 Hoffart, D.J. and Loeb, S.J. (2005) *Angew. Chem. Int. Ed.*, **117**, 901.
38 Li, J.-R., Bu, X.-H., Zhang, R.-H. (2004) *Inorg. Chem.*, **43**, 237 and references therein.
39 Hoffart, D.J. and Loeb, S.J. (2007) *Supramol. Chem.*, **19**, 89.

40 Tiburcio, J., Davidson, G.J.E. and Loeb, S.J. (2002) *Chem. Commun.*, 1282.

41 Mueller, U., Schubert, M., Teich, F., Puetter, H., Schierle-Arndt, K. and Pastre, J. (2006) *J. Mater. Chem.*, **16**, 626.

42 For a review on creating molecular machines in the crystalline state, see. Khuong, T.-A.V., Nuñez, J.E., Godinez, C.E. and Garicia-Garibay, M.A. (2006) *Acc. Chem. Res.*, **39**, 413.